8-2001

Synthesis of Nano-Structured Monoclinic $W0_3$ Particles

Zhixiang Lu

SYNTHESIS OF NANO-STRUCTURED MONOCLINIC WO_3 PARTICLES

By

Zhixiang Lu

B.S. Tongji University, 1995

A THESIS

Submitted in Partial Fulfillment of the

Requirements for the Degree of

Master of Science

(in Chemistry)

The Graduate School

The University of Maine

August, 2001

Advisory Committee:

Carl P. Tripp, Associate Professor of Chemistry, Advisor

Alice E. Bruce, Associate Professor of Chemistry

Touradj Solouki, Assistant Professor of Chemistry

SYNTHESIS OF NANO-STRUCTURED MONOCLINIC WO_3 PARTICLES

By Zhixiang Lu

Thesis Advisor: Dr. Carl P. Tripp

An Abstract of the Thesis Presented
in Partial Fulfillment of the Requirements for the
Degree of Master of Science
(in Chemistry)
August, 2001

The goal of this research is: 1) to develop synthetic methods for generating nano-sized particles of monoclinic WO_3 (m-WO_3) and 2) to use the high surface area of the nano-sized material in infrared spectroscopic studies of the reactions of gaseous molecules with the particulate surface. Two methods of making nano-structured monoclinic tungsten trioxide (m-WO_3) particles are investigated. In one method, the sol formation occurs in the presence of a solution containing chelating agents and in a second approach, the sol formation occurs in a water-in oil emulsion. Commercial m-WO_3 particles are approximately 1 micron in diameter (surface area of about 1.7 m^2/g). Particles of this size are not suitable for infrared studies. In contrast, particles produced using the chelating agents have surface areas of about 20 m^2/g whereas a higher value (about 45 m^2/g) is obtained via the emulsion method. Particles produced with either of these two alternate methods are shown to be suitable for infrared studies.

The focus of our synthetic effort centered on altering the conditions used in the condensation step of the reaction. In Chapter 3, we describe our results obtained using

chelating agents to slow down the rate of condensation and to impede particle growth. Specifically, acetic acid, oxalic acid dihydrate, and the mixture of the two were added at different concentrations and as a function of pH. Raman, XRD, FTIR, SEM, BET (N_2) were used to characterize the oxide product.

In chapter 4 we examine an alternative strategy using water-in-oil (W/O) emulsions. The condensation occurs in the aqueous phase inside a surfactant stabilized water droplet. In essence, the droplet is a micro-reactor limiting the size of the final WO_3 particles. Results obtained using different concentrations of tungstic acid and different molar ratio of water to surfactant (R) are discussed in this thesis. Our experiments show that the emulsion method leads to smaller particles than possible with using chelating agents.

In Chapter 5 we demonstrate the usefulness of the nano-sized particles for surface infrared studies. Specifically, we identify the changes that occur in the dehydroxylation/dehydration and Lewis acidity of the surface of monoclinic tungsten oxide (m-WO_3) powder as a function of evacuation temperature. It is shown that the m-WO_3 surface at room temperature contains both isolated and hydrogen bonded hydroxyl groups along with layer of adsorbed water and that both the surface hydroxyl groups and adsorbed water layer are eliminated by evacuation at 150 °C. Reactions with D_2O and pyridine show that the surface hydroxyl groups are accessible, ionic in character and easily displaced. However, the removal of the hydroxyl groups does not lead to exposure of underlying Lewis sites but rather to a reduction in the total number of adsorption sites on the surface. While dramatic changes in surface sites occur between ambient and 150 °C, there are few changes with evacuation between 150 °C and 400 °C.

ACKNOWLEDGEMENTS

Deep and sincere thanks are extended to my thesis advisor, Dr. Carl P. Tripp for his guidance, assistance and encouragement during my study and research at University of Maine. I am grateful to the other committee members, Dr. Alice E. Bruce and Dr. Touradj Solouki for their comments and guidance towards the completion of this thesis. I would also like to thank the funding from Navy Grant for the support and the help from Chemistry department and Laboratory for Surface Science and Technology.

A special thanks to Dr. Sofian Kanan for the help on the measurement of FTIR and the assistance concerning detailed work in the lab, especially during the beginning of my graduate study. I am equally grateful to Dr. Yang Xiang for his assistance concerning BET measurement and Ben McCool for the helpful discussion and suggestion. Thanks are extended to Dr. Scott Moulzoff for the assistance concerning the XRD study of WO_3, and Dr. Kelly Edward for the SEM measurement.

I would also like to thank the following students in our group: Brian Ninness, Anil Waghe, Shivashanker Bitla, Haiyan Li, William Tze, Young-Nam Cho, Kim Chung, Louis White, and Pei He. They gave me a lot of help and the friendship made me happy during my graduate work at University of Maine.

Finally I would like to thank my dear parents and my lovely wife Yuhao Wang for their love and encouragement.

TABLE OF CONTENTS

ACKNOWLEDGEMENTS.....ii

LIST OF TABLES.....vii

LIST OF FIGURES.....viii

Chapter

1. INTRODUCTION.....1

1.1 Metal oxide and nanostructure.....1

1.2 Sol-gel.....2

1.3 Tungsten trioxide sol-gel methods.....3

1.3.1 Tungsten alkoxide as precursor.....4

1.3.2 Acidification of sodium tungstate.....5

1.3.2.1 Precipitation of tungstic acid using HCl.....5

1.3.2.2 Ion-exchange resin.....6

1.4 Addition of organic chelating agents.....8

1.5 Emulsion used in sol-gel.....9

1.6 FTIR of WO_3 particles.....11

2. EXPERIMENTAL.....12

2.1 Materials.....12

2.2 Synthesis of tungsten trioxide.....13

2.2.1 Preparation of sol (H_2WO_4 solution) using ion-exchange resin.....13

2.2.1.1 Preparation of ion-exchange column.....13

2.2.1.2 Preparation of tungstic acid solution.....13

2.2.2 Synthesis of tungsten trioxide using chelating agents.....15

2.2.3 Synthesis of tungsten trioxide using an emulsion.....15

2.2.4 Calcination.....16

2.3 Characterization of tungsten trioxide powders.....17

2.3.1 Raman spectroscopy.....17

2.3.2 FTIR.....19

2.3.3 BET (N_2) surface area measurement of the WO_3 particles.....20

2.3.4 Scanning Electronic Microscopy (SEM) and X-ray Diffraction (XRD).....20

3. SYNTHESIS OF TUNGSTEN TRIOXIDE USING CHELATING AGENTS.....21

3.1 Introduction.....21

3.2 Sol-gel formation in water.....21

3.2.1 Direct sol from elutant.....21

3.2.2 Freeze-fracture of gel structures.....23

3.3 Dilution in water.....24

3.3.1 Effect of condensation time.....25

3.3.2 Calcination procedure.....26

3.3.3 Influence of pH on the surface area.....27

3.3.4 Influence of concentration of tungstic acid.....27

3.4 Formation of WO_3 in solutions of oxalic acid.....28

3.4.1 Concentration of tungstic acid 29

3.4.2 Effect of stirring time.....31

3.4.3 Influence of pH on the surface area.....31

3.5 Sol-gel reaction in solutions of acetic acid.....32

3.6 Sol-gel reactions in mixtures of oxalic acid and acetic acid.....33

3.7 Surface area vs particle size.....37

3.8 FTIR spectra 40

3.9 Conclusion.....42

4. SYNTHESIS OF TUNGSTEN TRIOXIDE PARTICLES USING W/O EMULSIONS.....43

4.1 Introduction.....43

4.2 Preparation of tungsten trioxide using W/O emulsion.....44

4.2.1 Preparation of the W/O emulsion.....44

4.2.2 Preparation of water/surfactant/toluene emulsion.....47

4.3 Results and discussion.....49

4.3.1 Emulsion using Span-60.....49

4.3.2 Emulsion using Span-80.....51

4.4 Conclusion.....52

5. IDENTIFICATION OF SURFACE SITES ON NANO-SIZED MONOCLINIC WO_3 POWDERS BY FT-IR SPECTROSCOPY.....54

5.1 Introduction.....54

5.2 Experimental section.....55

5.3 Results and discussion.....56

5.3.1 Dehydration of m- WO_3.....56

5.3.2 Dehydroxylation of m-WO_3.....63

5.3.3 Adsorption of pyridine.....64

5.4 Conclusion.....69

REFERENCES.....70

BIOGRAPHY OF THE AUTHOR.....75

LIST OF TABLES

Table 3.1 Direct sol-gel.....22

Table 3.2 Freeze fracture in liq. N_2.....24

Table 3.3 Effect of incubation time.....25

Table 3.4 Effect of temperature ramp.....26

Table 3.5 Effect of pH.....27

Table 3.6 Effect of dilution.....28

Table 3.7 Dilution in water.....30

Table 3.8 Concentration of oxalic acid 30

Table 3.9 Stirring time of gelation.....31

Table 3.10 Effect of pH in solution of oxalic acid dihydrate (OAD).....31

Table 3.11 Effect of pH of acetic acid solution.....32

Table 3.12 Sol-gel in solution of oxalic and acetic acids.....33

Table 4.1 Different amount of surfactant.....49

Table 4.2 Different concentration of tungstic acid.....50

Table 4.3 Different volume of tungtic acid.....50

Table 4.4 Change of surface area.....51

Table 4.5 Effect of the amount of Span-80.....52

LIST OF FIGURES

Figure 1.1 Structure of the droplet in the emulsion.....10

Figure 2.1 Ion exchange column.....14

Figure 2.2 Sol-emulsion-gel apparatus.....16

Figure 2.3 Raman spectra for m- WO_3 and hydrate.....18

Figure 3.1 Structure of WA_3 34

Figure 3.2 Structure of WB_6.....35

Figure 3.3 SEM pictures of WO_3 particles 38

Figure 3.4 FTIR (DRIFT) spectra for WO_3 powders.....41

Figure 4.1 Micelles and droplets in the emulsion.....45

Figure 4.2 Structure of Span-60 ($C_{24}H_{46}O_6$) 46

Figure 4.3 Span-80 ($C_{24}H_{44}O_6$)..... 46

Figure 5.1 Infrared spectra of the m-WO_3 powder evacuated at various temperatures 56

Figure 5.2 Desorption of water from m-WO_3 surface as a function of evacuated temperatures.....58

Figure 5.3 Infrared spectra of a) m-WO_3 powder and b) after addition of the D_2O vapor for 15 minutes at room temperature followed by evacuation for 2 minutes.....61

Figure 5.4 Infrared spectra of pyridine adsorbed at room temperature on m-WO_3 evacuated at (a) room temperature (b) 150 °C, and (c) 400 °C.....66

Chapter 1

INTRODUCTION

Our interest in studying gas phase reactions on the surface of m-WO_3 is based on its use in sensors for low level (ppb) detection of gaseous compounds. In a typical operating environment, the sensor will be exposed to a gas stream containing a myriad of compounds. Under these conditions it is difficult to decipher the complicated molecular chemistry that lead to a change in conductivity in m-WO_3 based sensors. Thus, the ability to identify and monitor surface species formed in gas phase reactions on m-WO_3 surfaces would aid the development of this technology.

WO_3 based metal oxide sensors are typically fabricated as a thin film oxide layer or as a powder anchored using a suitable binder to an underlying platform containing the electronic components. In both cases, the WO_3 thin film or powder is not amenable to surface studies by infrared spectroscopy. It is very difficult to detect the weak bands due to surface species because the thin films have very low surface area. Commercial powders are typically micron sized and exhibit high scattering of the infrared beam as well as relatively low surface area. By succeeding in fabricating nano-sized m-WO_3 particles we aim to reduce the scattering level and at the same time, increase the surface area to a point where surface infrared studies are possible.

1.1 Metal oxide and nanostructure

Metal oxide semiconducting films such as SnO_2[1,2], ZnO[3,4] and WO_3[5] have been used as the sensing element in gas detectors for many years. Upon exposure to gas, the films undergo dramatic changes in electrical conductivity and to a lesser extent changes

in mass and elasticity. These changes can be monitored and related to gas concentration either in a conductivity-type sensor (also known as a Taguchi sensor)[6] or in a surface acoustic wave (SAW) sensor device[7]. Grain-size reduction is one of the main factors enhancing the gas-sensing properties of semi-conducting oxides, and sharp increases in sensitivity are expected when the grain size becomes smaller than the space-charge depth[8]. Thus the use of nano-structured materials (both in powder and thin-film form) in gas sensors is generating much interest in the scientific community.[9-16] Success in generating nano-sized WO_3 particles could have a second application as material for powder based sensors.

1.2 Sol-gel

Sol-gel processing is a wet chemical route to synthesis of a colloidal suspension of solid particles or clusters in a liquid (sol), and subsequently to formation of a dual phase material of a solid skeleton filled with a solvent (wet gel) through sol-gel transition (gelation). When the solvent is removed, the wet gel converts to a xerogel through ambient pressure drying or aerogel through supercritical drying.

The use of the sol-gel process to produce sensitive films has attracted considerable research interest, because the sol-gel process offers a simple and versatile route to control nano-porous structures, enhancing the diffusion and interaction of the gas molecules with the film. The thickness, grain size, porosity, and composition of sol-gel derived films can be manipulated by the preparation conditions.

In the sol preparation, the precursors (either organic or inorganic) undergo two chemical reactions: hydrolysis and condensation or polymerization, typically with acid or

base as catalysts, to form small solid particles or clusters in a liquid (either organic or aqueous solvent). In this process an inorganic or organic molecular precursor $M(OR)_n$, a sol, is used as starting material, where M is a metal and (OR) an organic compound, respectively. The reaction can be utilized to provide oxides in the form of powders or a macromolecular network for use as thin films on other substrates.

In principle the sol-gel reaction can be written as:[17]

$$M(OR)_n + n/2H_2O \rightarrow MO_{n/2} + nROH \qquad \text{(Eq. 1.1)}$$

Organic additives are commonly used in sol-gel chemistry[18]. These additives can operate as stabilizers or reactive metal alkoxides[19,20] towards hydrolysis or as drying agents (such as dimethylformamide). These organic compounds and the by-products of sol-gel reactions can drastically modify the physical properties of the materials.

1.3 Tungsten trioxide sol-gel methods

Tungsten oxide (WO_3) thin films can be generated through several different methods, such as radio frequency sputtering[21], evaporation[22,23] or sol-gel process.[24] A "wet" chemical process of sol-gel has advantages of ease and flexibility in the fabrication of a variety of materials based on tungsten oxide framework. The literature on sol-gel tungsten oxides is almost entirely devoted to the formation of films on surfaces. The synthesis of the films can be divided into methods based on the hydrolysis of tungsten alkoxides and methods based on the acidification of alkali tungstates.

1.3.1 Tungsten alkoxide as precursor

The hydrolysis of metal alkoxides is, by far, the most common approach to metal oxide sol-gel synthesis. However, for tungsten oxide sol gels, the use of tungsten alkoxide precursors is not a common approach because the precursors are not readily available, have limited shelf life and are more expensive than alkali tungstates. Nevertheless, a number of sol-gel synthetic approaches to fabricate tungsten oxide sol-gel films have been reported.

WO_3 thin films have been prepared by mixing tungsten ethoxide $W(OC_2H_5)_6$ in n-butanol.[25,26] After ultrasonic agitation at room temperature for 1 hour, the prepared solution was spun onto a Pt substrate, then was exposed to air over night and annealed for 1 hour at a temperature higher than 400°C. The two steps of this process can be described as follows:

(i) Hydrolysis

$$W(OC_2H_5)_6 + 6H_2O \rightarrow W\text{-}(OH)_6 + 6C_2H_5OH \qquad \text{(Eq. 1.2)}$$

(ii) Condensation:

$$nW(OH)_6 \rightarrow (WO_3)_n + 3n.H_2O \qquad \text{(Eq. 1.3)}$$

An alternate approach is to freshly prepare a tungsten alkoxide precursor by reacting isopropanol with either tungsten oxychloride ($WOClO_4$)[27] or WCl_6[28]. Chloroalkoxides obtained from $WOCl_4$ or WCl_6 dilution with isopropanol (^{i}PrOH) give stable solutions with a viscosity suited to dip-coating processes.

$$WOCl_4 + x^iPrOH \rightarrow WOCl_{4-x}(O^iPr)_x + xHCl \quad \text{(Eq. 1.4)}$$

$$WCl_6 + x^iPrOH \rightarrow WCl_{6-x}(O^iPr)_x + xHCl \quad \text{(Eq. 1.5)}$$

Dip coated samples are left in air and hydrolysis and condensation occurs spontaneously with the ambient moisture to form stable films.

$$WOCl_{4-x}(O^iPr)_x + H_2O \rightarrow WO_3.2H_2O + HCl + {}^iPrOH \quad \text{(Eq. 1.6)}$$

$$WCl_{6-x}(O^iPr)_x + H_2O \rightarrow WO_3.2H_2O + HCl + {}^iPrOH \quad \text{(Eq. 1.7)}$$

1.3.2 Acidification of sodium tungstate

The most common approach to synthesizing tungsten oxide involves the acidification of sodium tungstate. Sodium tungstate is readily available and stable. The sodium tungstate is first converted to tungstic acid by either addition of HCl solution or generated by passing a sodium tungstate solution through an ion exchange resin.

1.3.2.1 Precipitation of tungstic acid using HCl

In the simplest method to make tungsten oxide hydrate[29], concentrated HCl solution was added into the solution of $Na_2WO_4.2H_2O$ in water drop-wise without stirring until the solution reached a pH~4 at a low temperature (0-5°C). A white precipitate formed and was washed several times.

$$Na_2WO_4 + 2HCl \rightarrow 2NaCl + H_2WO_4 \qquad \text{(Eq. 1.8)}$$

The precipitate was then dissolved in a concentrated solution of oxalic acid, and the transparent colloidal solution of tungstic acid formed.

The major advantage of this method is that formation of WO_3 occurs at room temperature. However, the solution is not adequately stable or pure for use in industrial production. The presence of Na^+ ions in the solution leads to mixture of sodium tungstates and tungsten oxide. Furthermore, the presence of counter anions, such as Cl^-, NO_3^-, SO_4^{2-}, strongly influence the polymerization process, and the final composition of the solid product[30,31].

1.3.2.2 Ion-exchange resin

The most widely used sol-gel method begins with the ion exchange of sodium tungstate at ambient temperature. Chemseddine et al.[32] have prepared stable WO_3 films using this ion-exchange process. A solution of $Na_2WO_4.2H_2O$ in water was passed through a protonated ion exchange resin, leading to a colloid solution of sodium and chloride free tungstic acid.[33]

$$Na_2WO_4 + 2H^+ \rightarrow 2\,Na^+ + H_2WO_4 \qquad \text{(Eq. 1.9)}$$

The sodium cation is removed and trapped by the resin. In the next step, the condensation (polymerization) of the H_2WO_4 results in a network of tungsten oxide.

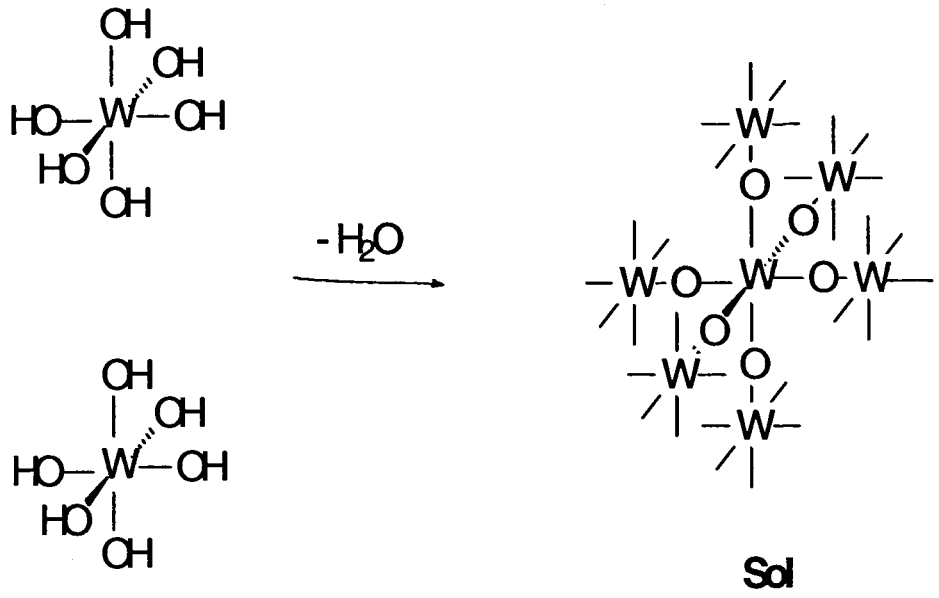

The polymerization in acidic conditions involves several stages[33], starting with formation of metal hydroxy complexes, formation of hydroxy polymers (olation), formation of oxobridges (oxolation) and finally a visible yellow tungsten trioxide hydrate $(WO_3.H_2O)_n$ solid product. Depending on the concentration and polymerization conditions, the sol may precipitate from the solution as individual particulates or form a stable gel.

The hydrated tungsten oxide is converted to a crystalline form by calcination at elevated temperature. A large weight loss and the endothermic peak at RT~200°C is found due to desorption of the physically trapped water and the small loss above 200°C is due to the dehydration of chemically trapped water (structural water).[34] The change of crystal structure of tungsten trioxide with the temperature has been widely studied by X-ray diffraction (XRD). The first crystallographic phase is triclinic occurring at 233-290°C, followed by monoclinic at 290-603°C, then orthorhombic at 603-993°C, and tetragonal above 993°C[35,36]. For sol-gel films, the material is amorphous and a crystalline

phase begins to appear at 200°C with a post-annealing cure. The films are completely crystallized at 350°C.[34] However, to make stable crystalline tungsten trioxide powders, calcination temperatures higher than 500°C are required. At temperatures below 500°C, the crystalline WO_3 slowly reverts back to its amorphous hydrated form.

In the formation of WO_3 particles, the growth of the hydrated tungsten oxide sol continues until the particle precipitates from solution. This occurs when the particles are approximately micron sized. To produce particles with high surface area (i.e., small size) it is necessary to inhibit the growth of the sol particulates. In addition, the aggregation of particles that occur during calcination step needs to be minimized. By controlling the condensation conditions and minimizing the aggregation of particles during calcination, it should be possible to obtain small WO_3 particles with high surface area. Two possible strategies at controlling the condensation/aggregation involve the use of organic chelating agents and W/O emulsions.

1.4 Addition of organic chelating agents

Chelating ligands such as oxalic acid[37,38], acetylacetone[39], and 2,4-pentanedione[40] have been used to generate stable WO_3 sol-gel films. The rate of condensation occurring between two WOH groups is reduced as the number of non-condensable chelating agents attached to the central W atom increases. The slower condensation or cure produces less stress between a sol-gel film and the substrate and this minimizes the cracking that occurs when the film is annealed at elevated temperatures. The chelating agents exchange with the OH^- ligands attached to the central W atom through a series of equilibria. The oxalate

anion is predominately a bidentate ligand and is more strongly bound to the central W atom than the monodentate acetate ion.

$$W(OH)_6 + xH_3CCOOH \rightleftharpoons W(OAc)_x(OH)_{6-x} + xH_2O \qquad \text{(Eq. 1.10)}$$

$$W(OH)_6 + yH_2C_2O_4 \rightleftharpoons W(C_2O_4)y(OH)_{6-2y} + 2yH_2O \qquad \text{(Eq. 1.11)}$$

The number of chelating ligands coordinated to the central W atom at any given time will depend on several factors affecting the position of the equilibria including the relative oxalate/acetate to $H_2WO_4.2H_2O$ [also depicted as $W(OH)_6$] initial concentration, pH and temperature.

Sun et al.[37,41] have recently reported the formation of nanocrystalline WO_3 thin films via a sol-gel method using oxalate chelating agents. Thus, it is expected that the chelating agents that bind to the $W(OH)_6$ will also inhibit the condensation, growth and aggregation of individual particles. Furthermore, it has been shown[38] that a bound oxalate remains on the hydrated tungsten oxide particle at temperatures up to 200°C. The presence of coordinated oxalate at these elevated temperatures should inhibit the reduction in surface area or aggregation of particles during the calcination step.

1.5 Emulsion used in sol-gel

The use of emulsions as microreactors to produce ultrafine particles was first described by Boutonnet et al.[42] They obtained ultrafine monodispersed metal particles of platinum, palladium, rhodium and iridium in the aqueous droplets of water-in-oil

emulsions. Water-in-oil emulsions have also been used to synthesize nanoparticles of metal borides[43], silver halides[44,45], $BaCO_3$[46], silica[47], TiO_2[48] and Al_2O_3.[49]

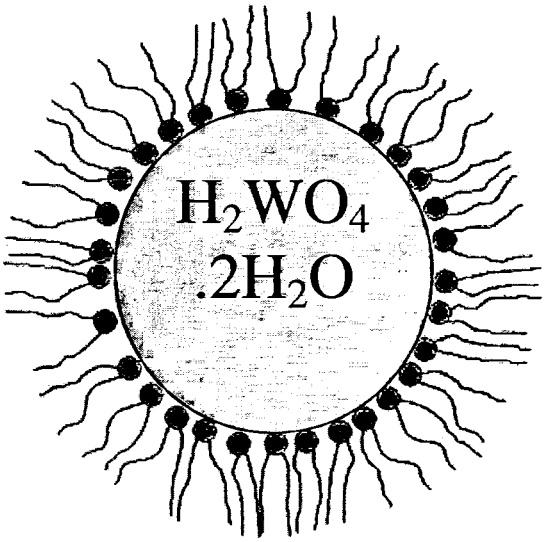

Figure 1.1 Structure of the droplet in the emulsion

The essence of the concept is shown in figure 1.1. The polymerization of the H_2WO_4 occurs in the aqueous phase inside a surfactant stabilized droplets. The growth and size of the particle is ultimately limited by the volume of the aqueous phase inside the droplet. The size of the droplet and concentration of the tungstic acid are key factors in determining particle size. This in turn, depends on several factors such as molar concentration ratios water/surfactant/oil [50-56]; nature and length of the alkyl chain of the oil[50-53], type of surfactant[52,53] and cosurfactant[55,56], temperature[50,54] and the nature and concentration of the electrolyte solubilized in the water droplets[50]. The studies of ternary and quaternary W/O emulsions show that a decrease in the surfactant or cosurfactant

chain length brings about an increase in droplet size and in the attractive inter-droplet interactions. The temperature and oil chain length have an opposite effect on these two properties.[57]

1.6 FTIR of WO_3 particles

Fourier-transform-infrared-spectroscopy (FTIR) measurements represent a very important tool for characterizing gas-sensing materials because they provide information both on the electronic properties of the powders and on the surface species formed in the presence of various testing gases.[58,59] For example, FTIR spectra of the WO_3 films show that presence of a very intense and broad absorption peak when an electron undergoes photoionization from monoionized oxygen vacancies (Vo^+) to the conduction band[60].

While there are numerous infrared studies devoted to monitoring the dehydroxylation/dehydration behavior as a function of temperature on many oxides[61], we are not aware of similar studies on monoclinic WO_3 (m-WO_3) powders. Typically, the identification of surface sites on metal oxide powders is largely based on the ability to detect infrared bands due to various hydroxyl groups (both from adsorbed water and surface M-OH modes) and by using the position of bands of adsorbed molecules such as pyridine to probe Lewis acid/Brønsted acid site densities. Bands due to adsorbed water on $WO_3 \cdot 2H_2O$ and NH_3 adsorption on sputtered tungsten oxide films have been detected,[62,63] but these studies were on amorphous WO_3 based material before crystallization into the stable monoclinic form.

Chapter 2

EXPERIMENTAL

In this chapter we describe the materials and general procedures used to synthesize and characterize the m-WO_3 particles. Each subsequent chapter also contains a brief experimental section describing the specific details related to that work. For example, in this chapter we describe the materials and details of the preparation of the ion exchange column and preparation of the oxalate/acetate solutions whereas the experimental section in Chapter 3 describes the specific reaction conditions.

2.1 Materials

Most chemicals were obtained from the Aldrich Chemical Company. These include the ion exchange resin DOWEX® 50WX2-200, sodium tungtate dihydrate (99%), oxalic acid dihydrate (99%), ammonium hydroxide (28%), as well and commercial monoclinic tungsten (VI) oxide powder (1-5 microns, 99.9%). The nonionic surfactants sorbitan monostearate (Span-60) and sorbitan monooleate (Span-80) used in the emulsion synthesis described in chapter 4 were also obtained from Aldrich Chemical Co. Inc, Milwaukee, WI.

Glacial acetic acid (99%) was obtained from Fisher Scientific, Pittsburgh, PA. Toluene (99.8+%) from Alfa Aesar, Ward Hill, MA. The water was doubly distilled deionized water (18 MΩ) obtained from a Millipore Filter System.

2.2 Synthesis of tungsten trioxide

2.2.1 Preparation of sol (H_2WO_4 solution) using ion-exchange resin

2.2.1.1 Preparation of ion-exchange column

Particular care was used to avoid trace Na^+ ions in generating H_2WO_4 as during the condensation step this would lead to mix products of WO_3 and sodium tungstates.[32,34] All glassware was ultrasonically cleaned with soap and water and rinsed thoroughly with the deionized H_2O three times before use. 35g of Dowex 50WX2-200 resin contains excess hydrochloric acid and is first washed with 400ml of DI water 3 times. Before the resin was transferred into a standard 50 ml buret, a small wad of cotton covered by a piece of Teflon film was inserted into the bottom of the buret. The 35g of the ion exchange resin was loosely packed in a standard 50 ml buret. Deionized water was passed through the column until the pH value of the water (measured using Litmus paper) exiting the column was 5~6. (The pH of double distilled water was 5.8) Alternatively, a solution of $AgNO_3$ could be used to test for residual Cl^- ions. However, we found the measurement of pH a simple and equally effective method to the use of $AgNO_3$.

2.2.1.2 Preparation of tungstic acid solution

A predefined amount of sodium tungstate dihydrate was dissolved in a 100ml volumetric flask of double distilled water. The amount of solute depended on the concentration used in the experiments and this typically was about 0.12 M.

The apparatus for collecting the H_2WO_4 solution is shown in figure 2.1.

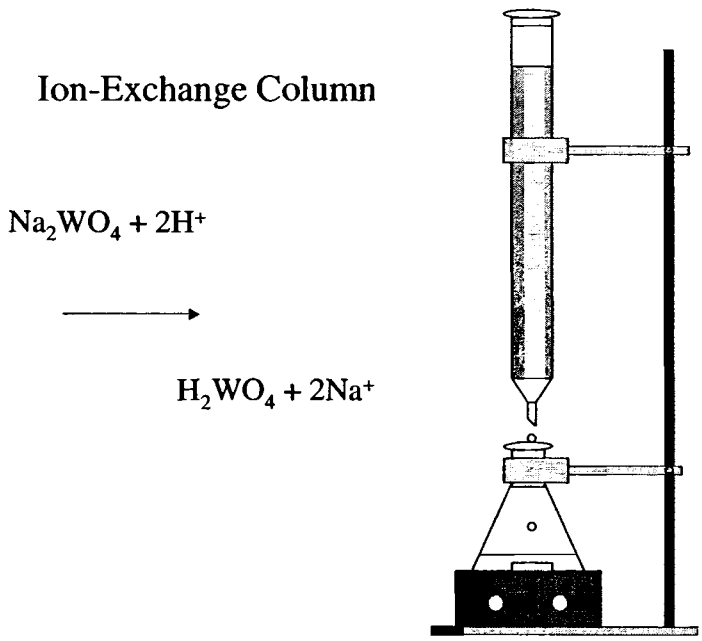

Figure 2.1 Ion exchange column

The solution of sodium tungstate dihydrate was added to a hydrogen ion-exchange column and eluted at a rate of 0.5 ml/min. The rate of elution depended on the concentration of the sodium tungstate dihydrate solution. The higher the concentration, the slower the elution rate. For example, a 0.24 M solution was eluted at a rate of 0.3 ml/min. When the elution rate is above 0.5ml/ml, the solution exiting the buret would include sodium ions. Experience has shown that there is a narrow operational range between solution concentration, amount of resin and elution rate. Using higher concentrations of Na_2WO_4 or less resin in the column leads to mixtures of WO_3 and sodium tungstate, whereas using more resin or slow elution rates clogged the column with polymerized WO_3 sol. Collection of the elutant began when the solution pH was 1.5 or lower.

2.2.2 Synthesis of tungsten trioxide using chelating agents

Detailed procedures are discussed in chapter 3. Solutions of oxalic acid dihydrate, glacial acetic acid or mixtures of both in the double distilled water were prepared before the sol of tungstic acid was added. In some cases, the pH value was adjusted with ammonium hydroxide solution. The tungstic acid solution was dripped into a stirred solution of the chelating agent(s). After 72 hours, the solution was heated to 150°C to remove the free water, and calcined at 500°C. A yellow powder of monoclinic tungsten trioxide was obtained.

2.2.3 Synthesis of tungsten trioxide using an emulsion

The elutant from the ion exchange column was dripped directly into the solution of non-ionic surfactant with low HLB (hydrophilic lipophilic balance) value in the organic solvent (see figure 2.2). The size of the water droplet depends on many factors such as stirring rate, surfactant concentration and surfactant type. Since the principal emulsifying agents are compounds containing both hydrophobic and hydrophilic, the HLB value is a geometric factor comparing the hydrophobic tail size to that of the hydrophilic headgroup. For a stable W/O emulsion, the HLB value for the surfactant should be in the range of 3~6. HLB values are tabulated for many surfactants and we selected the non-ionic surfactants, Span-60 and Span-80 in toluene. The structures of these two surfactants are shown in Chapter 4.

Strong mechanical agitation (~1000rpm) was applied in the first 30 minutes followed by a more gentle magnetic stirring for another 72 hours. While specific

experimental conditions are given in Chapter 4, the stirring rate (1000 rpm), HLB value of 3-6 and the range of surfactant/water/non-aqueous solvent concentrations used in our experiments give rise to emulsions with droplets of about 1micron in diameter. After 72 hrs of low speed stirring the sample sat without stirring for an additional 48 hrs to ensure that all remaining H_2WO_4 had reacted. The water was then extracted by evacuation, and the samples were then calcined at 500°C.

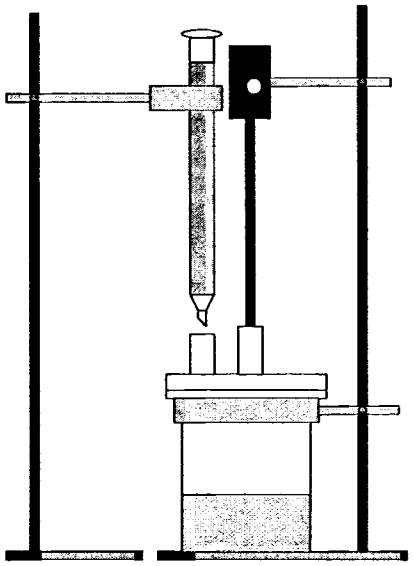

Figure 2.2 Sol-emulsion-gel apparatus

2.2.4 Calcination

To get stable monoclinic WO_3, the tungsten trioxide dihydrate obtained in sections 2.2.2 and 2.2.3 was calcined at 500°C. This step removed the physically adsorbed water and the structural water, as well to oxidize the organic addictives. Several heating protocols were tested. It was found that the higher the calcination temperature the

lower the surface area of the particle. Although monoclinic WO_3 was obtained at a minimum temperature of 400°C, the samples needed to be heated to at least 500°C. At temperatures below 500°C, the samples reverted to their amorphous hydrated form.

The heating rate was also an important parameter. A fast heating rate led to agglomeration of the water-laden particles and a reduction in surface area. To avoid size increase, the samples were first heated at 150°C for remove residual water. Samples were then heated at a rate of 10°C/min to 500°C and held at this temperature for 6 hrs followed by cooling to room temperature at a rate of 20°C/min.

The heating protocol for emulsion prepared samples differed slightly from that used with chelating agents. It was more difficult to oxidize the surfactants at the faster rate of 5°C/min. We found that a slower rate of 2°C/min was required followed by 6 hrs at 500°C and cooling at 20°C/min to room temperature. This initial slower rate did not change the surface area of the particles.

2.3 Characterization of tungsten trioxide powders

2.3.1 Raman spectroscopy

The calcined powders were first analyzed by Raman and infrared spectroscopy. Raman was used because of the ease in identifying characteristic bands for sodium tungstates, hydrated tungsten oxide and WO_3.[33,40,63-67] For all samples, characteristic sodium tungstate bands in 940-960 cm^{-1} range were not detected.[67] A spectrum of the hydrated tungsten oxide is shown in Figure 2.3 a, for comparison, Figure 2.3 b, c show the Raman spectra of a typical sample prepared either using the chelating agents or emulsion and the commercial powders.

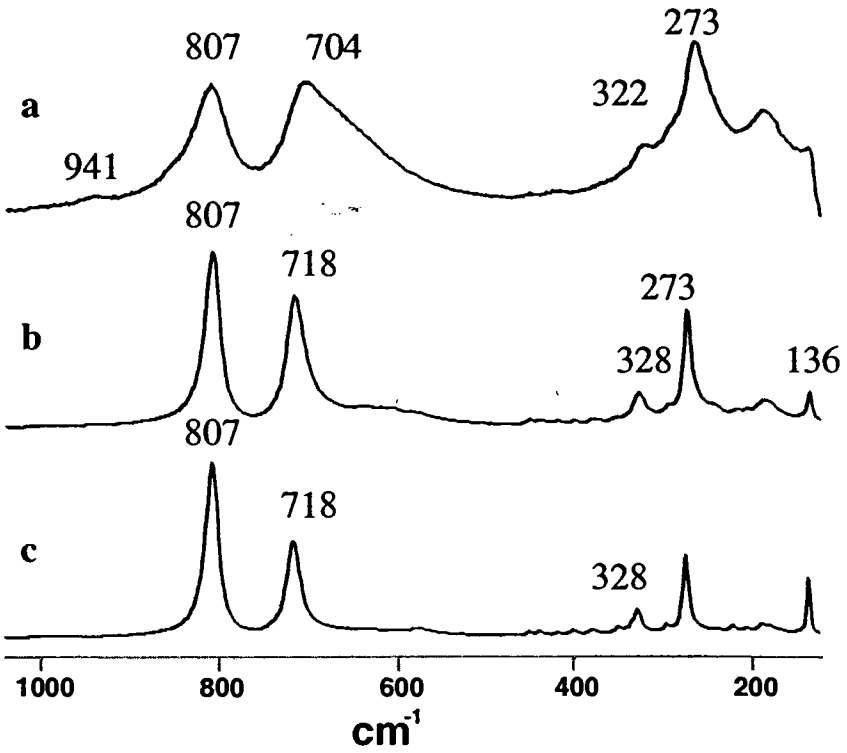

Figure 2.3 Raman Spectra for m- WO_3 and hydrate

a) hydrated tungsten oxide

b) typical sample using chelating agents or emulsion

c) commercial sample of m-WO_3

The similarity in the spectra of both samples b and c show that little, if any, hydrated tungsten oxide remains upon calcination. Major Raman bands at 807, 718 cm^{-1} (W-O stretching modes) and 273 and 136 cm^{-1} (W-O bending modes) in figure 2.3b and c are characteristic of monoclinic WO_3. Miyakawa et al.[67] have shown that the Raman bands at 810 and 715 cm^{-1} were observed for m-WO_3 and do not change as a function of temperature indicating the formation of a highly stable monoclinic crystalline WO_3 at

temperatures up to 500 °C. Raman spectra were collected using a Renishaw Raman Imaging Microscope System 1000. The system is equipped with a diode laser having λ_{ex} = 785 nm. Signal detection is achieved through the use of a sensitive charge coupled device (CCD) array detector.

2.3.2 FTIR

Infrared spectroscopy was used to detect the presence of residual surfactant or chelating agents (absence of C-H modes) and as a quick assessment of particle size and surface area. In brief, a smaller particle size exhibits less scattering of the infrared beam and is accompanied by more intense surface WOH and adsorbed water modes. FT-IR spectra were recorded on a Bomem MB-Series with a liquid N_2 cooled MCT detector. Typically 200 scans were co-added at a resolution of 4 cm^{-1}. Spectra were recorded in transmission using a thin film technique[68] or DRIFT using a Harrick Preying Mantis apparatus equipped with an environmental chamber.

Specific details on gas adsorption experiments are given in Chapter 5. Standard vacuum line techniques were used for the gas phase experiments. In pyridine adsorption experiments, difference spectra are plotted where the reference spectrum is recorded using the thin film m-WO_3 evacuated at room temperature. Therefore, positive bands are due to bonds that formed on the surface and negative bands represent bond removal from the surface due to pyridine adsorption. The results obtained on the synthesized nano-sized particles were compared to the results obtained with commercial m-WO_3 powder.

2.3.3 BET (N_2) surface area measurement of the WO_3 particles

Burner-Emmett-Teller (BET) surface area measurements were recorded on a Gemini 2360 Surface Area Analyzer Micromeritics instrument. The surface area measurement in this system is based on the volume of nitrogen uptake by a known amount of sample at liquid nitrogen temperature. Samples were degassed at 150°C for 4 hours and the pressure of nitrogen gas was maintained at about 25~30 psi, as was the pressure for helium gas. The data for the surface area was in (x-0.2, x+0.2) m^2/g with confidence 95%.

2.3.4 Scanning Electronic Microscopy (SEM) and X-ray Diffraction (XRD)

Representative samples were analyzed for crystallization by powder X-Ray diffraction (XRD) and particle size/shape by Scanning Electron Microscopy (SEM).

SEM graphs were taken on AMRay 1000. This instrument has a resolution of 7 nm, a magnification range of 20-100,000X, and an accelerating-voltage range of 1-30 kV. The powders were mounted on a eucentric goniometer stage, which enabled both tilt and rotation about the viewing axis.

All XRD patterns showed that the calcinated WO_3 was monoclinic in crystalliztion. XRD measurements were performed using a X2 Advanced Diffraction System which was equipped with a copper anode and a single crystal lithium doped silicon peltier detector which has a 100% energy absorption from 2-20 Kev with a Beryllium window thickens of 0.005 inches.

Chapter 3

SYNTHESIS OF TUNGSTEN TRIOXIDE USING CHELATING AGENTS

3.1 Introduction

An exhaustive search for a commercial source of high surface area m-WO_3 particles met with little success. The best commercial particles had measured surface areas of 1.7 m^2/g and as we show in this chapter, are not suitable for surface infrared studies. It is estimated that a particle size reduction of at least a factor of 10 (i.e., about 20 m^2/g) is desired for our infrared studies. Given this requirement, our first attempt at producing smaller m-WO_3 particles centered on methods of altering the condensation conditions in water. This is the simplest synthetic approach and the results obtained would serve as a benchmark for our synthetic work using of chelating agents or emulsions. In the chapter, we present our results obtained from the synthesis of m-WO_3 particles in water and compare these to the results obtained when using solutions of oxalic acid dihydrate, acetic acid, and mixtures of these two compounds. Parameters that were varied include concentration of the tungstic acid in the solution, pH, stirring rate and calcination conditions. The materials have been characterized with FTIR, Raman, XRD, SEM, BET (N_2).

3.2 Sol-gel formation in water

3.2.1 Direct sol from elutant

The simplest approach is to collect the elutant exiting the ion exchange column in a beaker and allow the polymerization to proceed with stirring. A solution of 0.12 M

$Na_2WO_4.2H_2O$ was passed through the ion-exchange column and the tungstic acid collected was simply allowed to polymerize at room temperature. After about 2hrs, a white gel formed and this gel was stable for more than 60 hours. During this time, the color of the gel gradually changed white to yellow. The gel then phase separated forming precipitated yellow particles leaving a clear layer of water on top. The Raman spectrum of the yellow particles showed that this material was hydrated tungsten trioxide. The water was decanted, and the sample was heated to 500°C at a ramp of 5°C/min. The sample was annealed at 500°C for 6 hours and then cooled to room temperature at a decreasing rate of 20°C/min. The calcination steps are important in dictating particle size. The calcination protocol used above is repeated throughout this thesis. Section 3.3.2 describes the effect of different calcination procedures and it is found that the above protocol leads to particles with the largest surface areas.

Samples were synthesized using two different incubation times. The calcination of sample A1 occurred at 72 hr gelation whereas sample A2 was allowed to gel for 102 hrs. The surface area of these two samples is listed in Table 3.1 and both Raman and XRD spectra showed that both samples were monoclinic WO_3.

Table 3.1 Direct sol-gel

Sample	Gel time (hr)	Surface area (m^2/g)
A1	72	5.0
A2	102	5.1

There was little difference in surface areas for A1 and A2 samples showing that a 72 hr incubation is sufficient. While the surface area is below our requirement, it is a factor of 3 higher when compared to the surface area of the commercial powder.

3.2.2 Freeze-fracture of gel structures

The above experiments showed that longer gel time than 72 hrs did not lead to a change in particle size. However it was not known if shorter gel times lead to larger particles. In the next set of experiments we combined shorter gel times with a second processing step of immersion in liquid N_2. Immersion of a gel structure in liquid N_2 can lead to a variety of structured materials[69]. These structures depend on the structure of the gel network and the rate at which the temperature is lowered. A rapid or "shock" reduction in temperature leads to a shattering of the gel structure and smaller particulate fragments. In essence, the rapid expansion of the ice in the hydrated gel network fractures the gel structure.

A 0.12M tungstic acid solution from the ion-exchange column was collected in a beaker. Aliquots were extracted at different gel incubation times, placed in a test tube and cooled rapidly by immersing liquid N_2 for 10 minutes. It required about 1 minute to immerse a tube containing the sample into the liquid nitrogen. After 10 minutes, the tube was removed and allowed to warm to ambient conditions. The gel was destroyed by the rapid cooling process and yellow particles appeared at the bottom of the test tube. Seven samples were prepared in this manner, which differ in the time extracted from the beginning of the gelation period. Each sample was then calcined to 500°C as described in

the previous section. The measured surface areas of these materials are presented in Table 3.2.

Table 3.2 Freeze Fracture in Liq. N_2

Sample	Incubation time before immersion in liq. N_2 (hr)	Surface Area (m^2/g)
B1	12	3.8
B2	24	6.2
B3	36	6.8
B4	48	7.5
B5	60	7.2
B6	72	4.4
B7	102	6.8

The data shows that a slight improvement in surface area is obtained with freeze-fracturing in liquid N_2. Samples are generally between 6-7 m^2/g and this is above the value of 5 m^2/g obtained for the data shown in Table 3.1. Furthermore, the data shows that there is little variation in particle size with gel times less than 72 hrs.

3.3 Dilution in water

In our experiment, we dripped the elutant from the ion exchange column into beakers containing water. This is, in effect, a dilution in concentration and is often used in sol-gel synthesis as a method for reducing particle size. A less dense gel structure is expected at lower precursor concentrations.

3.3.1 Effect of condensation time

A 0.12M sodium tungstate solution was added to the ion exchange column and 20 ml of the tungsten acid exiting the column was directly added to a container containing 400 ml of water. The samples were stirred for 24, 48,72 and 102 hrs and then dried and calcined at 500°C. The measured surface area of these 4 samples is shown in Table 3.3. The surface areas of all 4 samples showed little variation and were slightly lower than those obtained without dilution in water.

Table 3.3 Effect of incubation time

Sample	V-elutant (ml)	H_2O (ml)	Time (hr)	Surface Area (m^2/g)
C1	20	400	24	3.1
C2	20	400	48	4.0
C2	20	400	72	3.3
C4	20	400	102	2.7

Even though a dilution in water yielded smaller surface areas, we continued with additional experiments with dilution in order to explore alternative conditions (i.e., pH) and because this information is need as control experiments for the work using chelating agents

3.3.2 Calcination procedure

The post-processing curing of the hydrated tungsten oxide is needed to convert this material to a monoclinic WO_3. This step plays a role in dictating particle surface area. In the sol-gel synthesis, the higher the calcination temperature, the greater the sintering and thus the higher the reduction in particle surface area. In our case, we find a change in surface area (factor of 2) by simply raising the calcination temperature from 500 to 550°C. However, at temperatures below 500°C the conversion to m-WO_3 is not complete and with time, the material reverts back to an amorphous hydrated tungsten oxide. Therefore all calcination was done at 500°C.

The temperature ramp also affects particle size. A slower ramp is generally preferred, as a fast temperature rise often leads to a collapse of the network structure and a reduction in surface area. An example of the effect of temperature ramp rate on surface area is shown in table 3.4. Samples of tungsten trioxide hydrate were heated after a 72 hour gelation period. Calcination occurred at 3 different temperature ramp rates.

Table 3.4 Effect of Temperature Ramp

Sample	V-elutant (ml)	H_2O (ml)	Temp Ramp (°C/min)	Surface Area (m^2/g)
D1	20	400	5	3.3
D2	20	400	10	2.7
D3	20	400	20	2.1

It is shown that the slower temperature rate of 5°C/min gave the highest surface area. Given this result, we fixed the heating protocol to 500°C at a 5°C/min ramp.

3.3.3 Influence of pH on the surface area

The sol-gel condensation reaction for most oxides are acid catalyzed and therefor choice of pH could influence the surface area obtained for the m-WO_3 particles. The samples shown in Table 3.5 were prepared by diluting the sol in 1000 ml of double distilled water. For sample E1, the gelation occurred at the natural pH at 3.1, whereas for sample E2 the pH was adjusted with ammonium hydroxide to 7.0. The samples were stirred for a period was 72 hrs and then calcined at 500°C. From this data it is clear that the pH does not significantly alter the particle surface area.

Table 3.5 Effect of pH

Sample	V-elutant (ml)	H_2O (ml)	pH	Specific surface area (m^2/g)
E1	20	1000	3.1	2.8
E2	20	1000	7	3.3

3.3.4 Influence of concentration of tungstic acid

The effect of dilution on final particle surface area was examined (see Table 3.6). 20 ml of the elutant (0.12M) was dripped into various quantities of water ranging from 200 ml to 1000 ml. The solutions were stirred (300 rpm) for 72 hrs and the precipitated

particles were then calcined at 500°C. The dilution of the tungsten oxide had little effect on the final surface area.

Table 3.6 Effect of dilution

Sample	V-elutant (ml)	H_2O (ml)	Surface area (m^2/g)
F1	20	200	3.2
F2	20	400	3.2
F3	20	1000	2.8

The combined results obtained from condensation of the tungsten oxide in water shows that the particle surface areas varies from about 2.5 to 7.5 m^2/g depending on specific reaction conditions. While this is an improvement over the commercial particles, it is below the needed area for surface infrared measurements. The next level of improvement in surface area will not likely arrive using water only sol-gel procedures.

3.4 Formation of WO_3 in solutions of oxalic acid.

Chelating ligands such as oxalic acid[37,38], acetylacetone[39], and 2,4-pentanedione[40] have been used to generate stable WO_3 sol-gel films. However, the use of chelating agent as a way of fabricating high surface area WO_3 particulates has not been reported. In this case, it is expected that the coordination of the tungstic acid sol with the oxalate and acetate ligands will slow the condensation reaction as well as inhibit the growth of larger hydrated tungsten oxide particles.

Tungstic acid (0.12M) was prepared using the ion-exchange column. The solutions of oxalic acid, acetic acid or acetic/oxalic acid mixtures in water were prepared before the elutant was added. The addition of the tungstic acid to the solution containing the chelating agent did not lead to formation of precipitate or gel. The solutions were clear at all times. After stirring for 72 hrs the solutions were dried in an oven at 150°C. This produced a white crystalline solid that was predominately excess oxalic or acetic acid. The subsequent calcination at 500°C gave the characteristic yellow powder of m-WO_3.

3.4.1 Concentration of tungstic acid

In the first experiment we synthesized WO_3 particles in solutions in which the elutant/oxalic acid amount remained constant and the volume of water was altered. This examines the effect of dilution. First, there is a significant increase in surface area compared with all attempts using water only synthesis. Particles of this surface area do now meet our requirement for surface infrared studies. It appears that the higher the dilution the higher the surface area of the particle. This is opposite to the trend observed for water only based systems. Thus, a reduction in rate of condensation does lead to smaller particles. The coordinated oxalate ion reduces the number of WOH sites available for condensation and a decreased concentration of tungstic acid leads to fewer collisions between molecules per unit time.

Table 3.7 Dilution in water

Sample	V-elutant (ml)	Oxalic acid (g)	H_2O (ml)	Surface Area (m^2/g)
G1	20	30	100	17.2
G2	20	30	200	18.5
G3	20	30	1000	19.5

Next we varied the concentration of oxalic acid. Sun et al.[70] reported that a higher concentration of oxalic acid led to smaller crystal of tungsten oxide hydrate in sol-gel films. In all cases, (see Table 3.8) samples with acceptable surface areas for infrared studies were obtained. Changing the oxalate concentration had little influence on particle size. Given the level of excess oxalate crystals in the dried sample, it is likely that all samples have excess quantity of oxalate ions present.

Table 3.8 Concentration of oxalic acid

Sample	V-elutant (ml)	Oxalic acid (g)	H_2O (ml)	Surface Area (m^2/g)
H1	20	10	400	19.4
H2	20	20	400	18.3
H3	20	40	400	17.6
H4	20	50	400	19.1

3.4.2 Effect of stirring time

Table 3.9 Stirring time of gelation

Sample	V-elutant (ml)	Oxalic Acid (g)	H_2O (ml)	Time (hr)	Surface area (m^2/g)
I1	20	30	400	24	19.0
I2	20	30	400	48	15.1
I3	20	30	400	72	15.7
I4	20	30	400	102	16.3

Again the robustness of this method is demonstrated with the data obtained with different stirring times. The samples show consistent values for surface areas.

3.4.3 Influence of pH on the surface area

The number of oxalate ions available to coordinate to the tungstic acid is pH dependent. The pK_{a1} and pK_{a2} values for the diacidic oxalic acid are 1.23 and 4.17, respectively. However, the particle surface area for a sample prepared at pH 1.22 and pH shows little difference. The natural pH value for sample J1 after addition of the elutant is about 1.2 and the adjustment to pH 7.0 was done by addition of ammonium hydroxide.

Table 3.10 Effect of pH in solution of oxalic acid dihydrate (OAD)

Sample	V-elutant (ml)	H_2O (ml)	OAD (g)	pH	Specific surface area (m^2/g)
J1	20	1000	20	1.2	16.4
J2	20	1000	20	7.0	18.0

The insensitivity to pH arises from the relatively low pK_{a1} value of oxalic acid, which ensures the presence of oxalate anions at relatively low pH values. This contrasts with the pH dependence that is shown in the next section for the weaker acetic acid.

3.5 Sol-gel reaction in solutions of acetic acid

Another chelating agent, acetic acid was also used in the synthesis of tungsten trioxide powders. The surface area obtained using acetic acid produces much lower surface areas than obtained with oxalic acid (see Table 3.11). The acetate is predominately a monodentate ligand and is more weakly bound the W atom than the bidentate oxalate ion. At low pH the acetic acid has no effect on the powder surface area. The surface areas are similar in value to those obtained with water only systems. At this low pH, yellow particles formed in solution and precipitated out from solution. This is because acetic acid is a weak acid with a pK_a value of 4.74. At a pH of 2.2, acetic acid is predominately in a molecular form with few acetate ions in solution. In essence, the acetic acid behaves as a spectator molecule in the sol-gel reaction. However, at pH 7, we obtain a dramatic increase in particle because at this pH, the acid is ionized and the acetate ions coordinate with the W atom. Nevertheless, the surface area obtained with acetic acid below those obtained with oxalate ions by a factor of 2.

Table 3.11 Effect of pH of acetic acid solution

Sample	V-elutant (ml)	H_2O (ml)	Acetic acid (ml)	pH	Specific surface area (m^2/g)
K1	20	1000	40	2.28	4.0
K2	20	1000	40	7.0	9.3

3.6 Sol-gel reactions in mixtures of oxalic acid and acetic acid

Samples prepared from the solution of the mixture of oxalic acid and acetic acid were also studied. As before, a 0.12 M tungstic acid was added directly from the ion exchange column into the solution of the acids. Reactions were performed at a pH of 1.19 (the natural pH of the solution) and at pH value of 7.0 by addition of ammonium hydroxide.

Table 3.12 Sol-gel in solution of oxalic and acetic acids

Sample	V-elutant (ml)	H_2O (ml)	Acetic acid (ml)	Oxalic acid (g)	pH	Specific surface area (m^2/g)
L1	20	1000	40	20	1.19	17.4
L2	20	1000	40	20	7.0	22.4

The surface area obtained for sample L1 was 17.4 m^2/g, close in value to the samples prepared from oxalic acid solutions. This is expected, as at the low pH the acetic acid is a spectator molecule. When pH was adjusted to 7.0, both oxalate and acetate ions can coordinate to the W atoms of the tungstic acid. Clearly, the oxalate will dominate as this is a stronger chelating agent than the acetate ion.[38] However, repeated experiments always show a slightly higher surface area are obtained when using oxalate/acetate mixtures than samples obtained with only oxalate.

We recall that the coordination of oxalate (A^{2-}) or acetate ions (B^-) to the central W atom occurs through a series of competitive equilibrium reactions.

$$W(OH)_6 + A^{2-} \underset{}{\overset{K_{A1}}{\rightleftharpoons}} W(OH)_4A + 2OH^- \qquad \text{(Eq. 3.1)}$$

$$W(OH)_4A + A^{2-} \underset{}{\overset{K_{A2}}{\rightleftharpoons}} W(OH)_2A_2 + 2OH^- \qquad \text{(Eq. 3.2)}$$

$$W(OH)_2A_2 + A^{2-} \underset{}{\overset{K_{A3}}{\rightleftharpoons}} WA_3 + 2OH^- \qquad \text{(Eq. 3.3)}$$

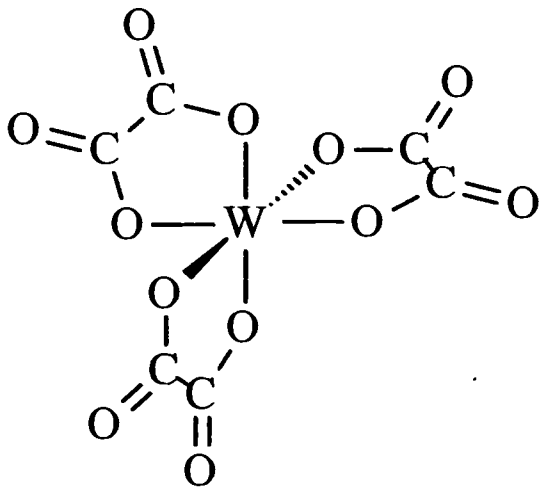

Figure 3.1 Structure of WA_3

$$W(OH)_6 + B^- \rightleftharpoons^{K_{B1}} W(OH)_5B + OH^- \quad \text{(Eq. 3.4)}$$

$$W(OH)_5B + B^- \rightleftharpoons^{K_{B2}} W(OH)_4B_2 + OH^- \quad \text{(Eq. 3.5)}$$

$$W(OH)_4B_2 + B^- \rightleftharpoons^{K_{B3}} W(OH)_3B_3 + OH^- \quad \text{(Eq. 3.6)}$$

$$W(OH)_3B_3 + B^- \rightleftharpoons^{K_{B4}} W(OH)_2B_4 + OH^- \quad \text{(Eq. 3.7)}$$

$$W(OH)_2B_4 + B^- \rightleftharpoons^{K_{B5}} W(OH)B_5 + OH^- \quad \text{(Eq. 3.8)}$$

$$W(OH)B_5 + B^- \rightleftharpoons^{K_{B6}} WB_6 + OH^- \quad \text{(Eq. 3.9)}$$

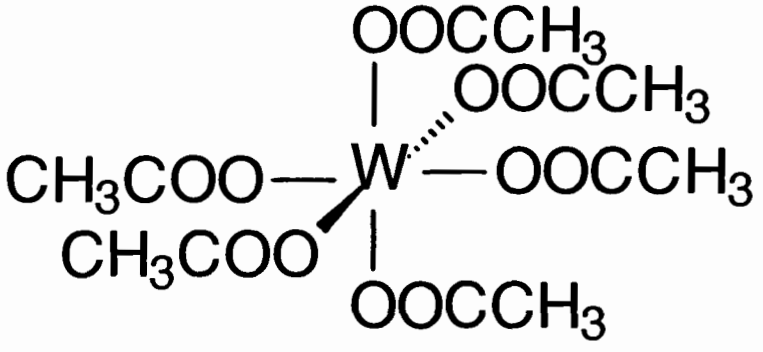

Figure 3.2 Structure of WB_6

This is an oversimplification of the reaction both oxalate and acetate can bind monofunctionally or difunctionally and the oxalate could bridge between two W atoms. In addition, the tungstic acid $W(OH)_6$ would in parallel undergo condensation . The acids

themselves are involved in pH dependant equilibria with the number of anions present in solution. For the diprotic oxalic acid this is:

$$H_2A \rightleftharpoons H^+ + HA^- \rightleftharpoons H^+ + A^{2-} \qquad \text{(Eq. 3.10)}$$

whereas for the monoprotic acetic acid the equilibrium is:

$$HB \rightleftharpoons H^+ + B^- \qquad \text{(Eq. 3.11)}$$

At pH = 7 both acids would exist in ionic form and both A^{2-} and B^- ions would be present in solution.

It is not clear as to the underlying reason for higher surface area particles obtained with mixed oxalate and acetate ions. In general, a higher surface area when there is a higher average number of coordinated ligands per W atom. Statistics dictate that the displacement of OH^- by either a acetate or oxalate reduces the probability that two tungstic acids will collide and undergo a condensation reaction. It is also observed that the divalent oxalate (A^{2-}) leads to higher surface area particles than found with acetate ions (B^-). The A^{2-} ion is more strongly bound to the W atom, is less likely to be displaced by an OH^-. Therefore, one possible explanation for a higher surface area is observed with oxalate/acetate is that the average number of coordinated chelating ligands per W atom is slightly higher with the mixture. The maximum number of A^{2-} surrounding a W atom is 3

but $K_{A1} > K_{A2} > K_{A3}$ so that each additional coordinated oxalate is more weakly bound to the W atom. With a monodentate B^- species present there is a possibility that there would be additional 5 coordinate W [i.e. $WA_2B(OH)$] species that would not be

possible with oxalate only. This would give, on average, a higher number of coordinated ligands per W atom and lead to higher surface area particles.

3.7 Surface area vs particle size

For each sample we measured BET surface area and from this value a average particle size can be computed. Assuming a spherical particle the relationship between surface area (SA) and particle diameter is:

$$SA = 6/ (Dia. \times density) \qquad (Eq. 3.12)$$

The density of WO_3 is 7.2 g/cm^3 and thus a SA value of 20 m^2/g gives a particle diameter of about 40 nm. However, this measurement does not differentiate between external and pore area. For infrared studies there is a need for both high surface area and small particle size. For example, it is easy to record transmission spectra of a 300 m^2/g fumed silica (nonporous, 10 nm) whereas a 300 m^2/g silica gel is difficult because the gel scatters the infrared beam. The scattering obtained with silica gels is due to the larger particle size. The silica gels are typically micron diameter in size and the high surface area arises because these materials are highly porous. Thus, surface area measurements are not sufficient to determine the differences in particle size. Therefore, we periodically recorded SEM pictures of our synthesized WO_3 particles to examine particle size. In all cases, there was good agreement with the calculated particle diameter based on surface area measurements and SEM pictures.

Figure 3.3 SEM pictures of WO_3 particles
a. Commercial Sample

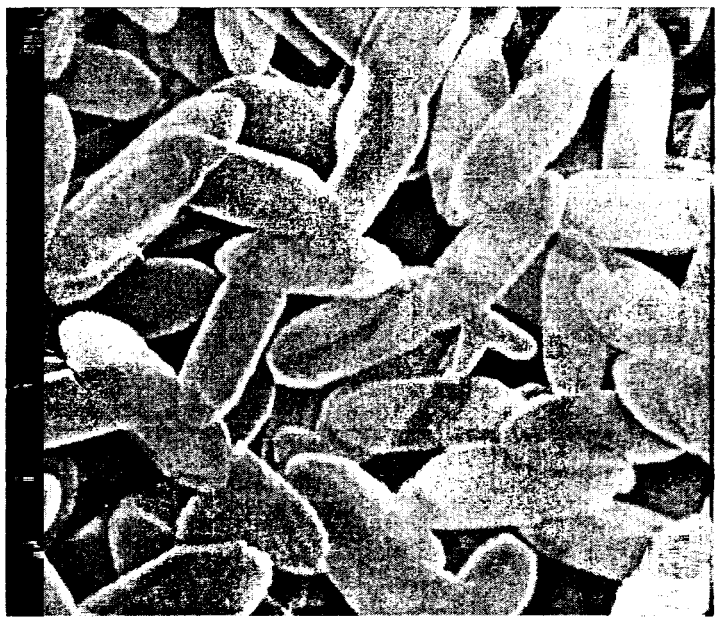

b. From Acetic acid

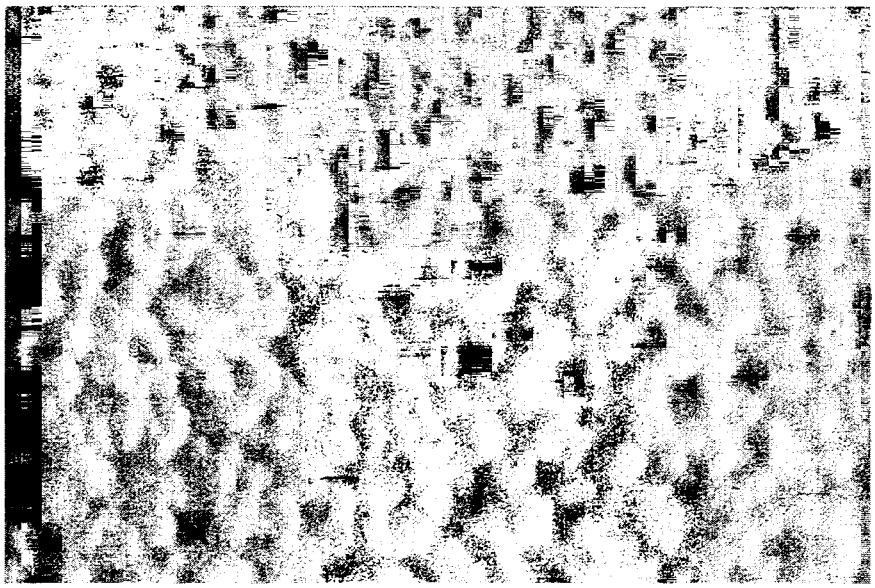

1μm

c. From oxalic acid ($18m^2/g$)

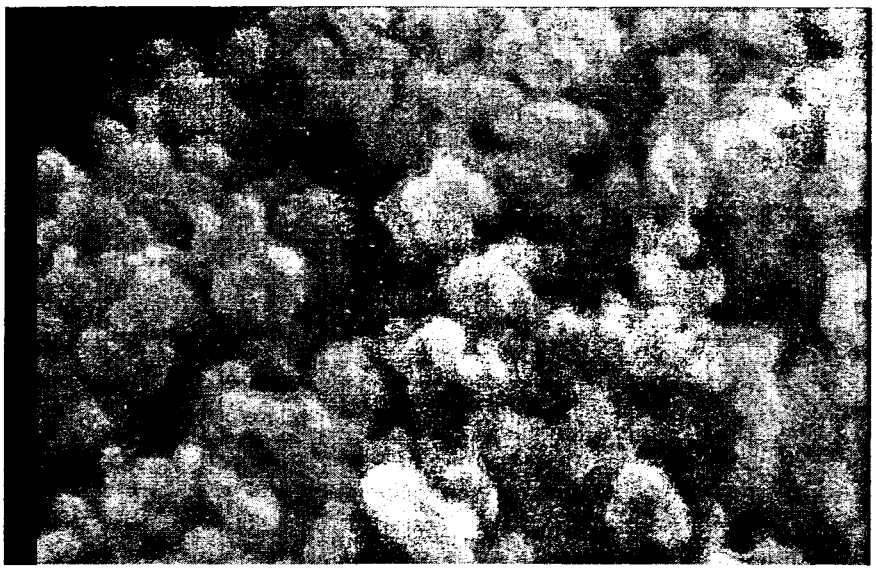

1μm

d. From oxalic acid ($18m^2/g$)

Figure 3.3 a, b, c and d show the SEM photographs for commercial m-WO_3 powders and those prepared via the sol-gel method using the acetic acid ($4m^2/g$) and oxalic acid ($18m^2/g$). The SEM results show that the oxalate prepared m-WO_3 samples were found to be nano-sized particulates with primary particle size of 30-50 nm which is consistent with the size computed from surface area data.

3.8 FTIR spectra

The principle aim of our synthetic effort is to produce high surface area m-WO_3 particles for use in infrared studies of reactions on the oxide surfaces. The DRIFT spectra of a medium range area (about 18 m^2/g) powder synthesized using oxalate chelating agent and that recorded for commercial powder is shown in Figure 3.4. The higher surface area enable detection of bands due to surface OH and adsorbed water in the 3700 to 3100 cm^{-1} region. Specifically, the broad band at 3450 and 3692 cm^{-1} are due to various O-H stretching modes and a sharp mode at 1620 cm^{-1} is the H_2O bending mode. In contrast, no bands were observed in the region 3400-3700 cm^{-1}or at 1620 cm^{-1} (see Figure 3.4a) in the DRIFT spectrum of the commercial samples. The relative amount of water adsorbed on the surface (and hence the relative surface areas of the powders) can be measured by ratioing the intensities of the 1622 cm^{-1} water bending mode to that of the surface overtone mode at 2063 cm^{-1}. In recording spectra for various samples (not shown), it is found that the relative amount of water adsorbed agreed with the trend in measured BET surface area and follows the order: emulsion > oxalic/acetic acid mixtures > oxalic acid > acetic acid > sol-gel in water only > commercial WO_3 powders.

There is one additional difference between the spectrum of commercial powders and the nano-fabricated samples. The infrared spectrum for the nano-sized WO_3 also shows a sharp band for CO_2 at 2342 cm^{-1} and this band is not present in commercial samples or those prepared using water only. This band did not reduce or change upon evacuation and elevation of the temperature up to 400 °C and represents trapped CO_2 formed during the oxidation of the chelating agent.

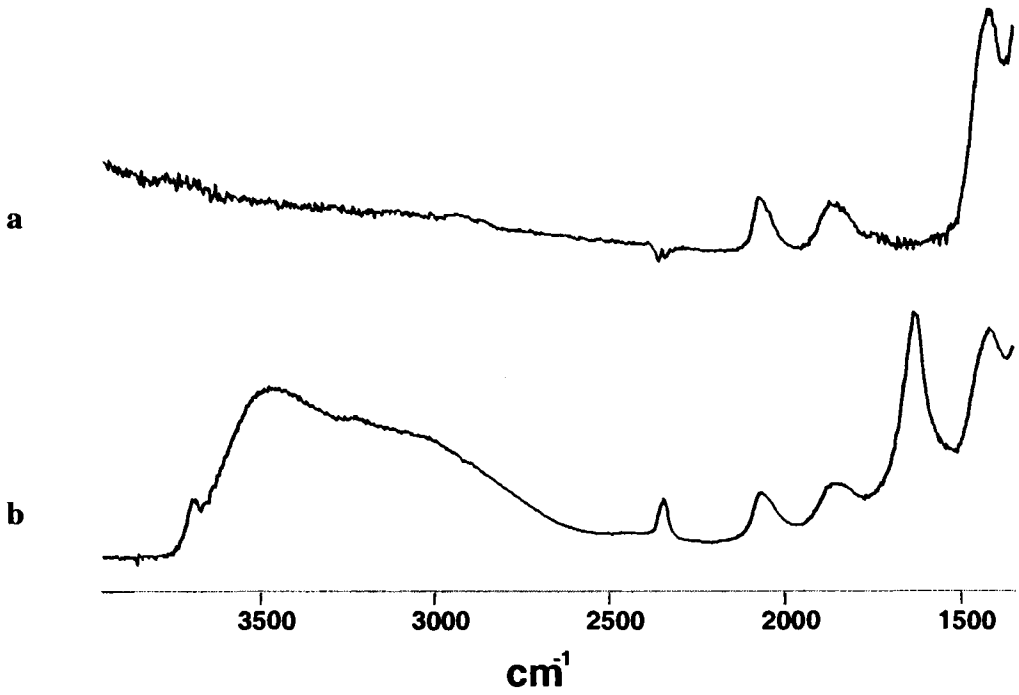

Figure 3.4 FTIR (DRIFT) spectra for WO_3 powders

a. Commercial particles

b. Synthesized using oxalate chelating agents

3.9 Conclusion

Synthesis of m-WO3 in water produces particles with surface areas between 2-7.5 m^2/g. While not suitable for surface infrared studies, these particles are an improvement over the $1.7m^2/g$ surface area of commercial material. By using oxalic acid or mixtures of oxalic acid and acetic acid, the surface area is increased to approximately $20m^2/g$. Particles synthesized using only acetic acid had surface areas lower by a factor of 2 than those obtained with oxalic acid. While surface infrared studies are difficult with commercial particles, it is easy to detect infrared bands due to surface species on particles with surface areas of about $20m^2/g$.

Chapter 4
SYNTHESIS OF TUNGSTEN TRIOXIDE PARTICLES USING W/O EMULSIONS

4.1 Introduction

In chapter 3 we reported success in achieving our goal of fabricating m-WO_3 particles with surface areas of at least 20 m^2/g suitable for infrared surface studies. The question remained as to whether this is the limit or is it possible to prepare material with even higher surface area. Any further increase in surface area beyond this value would directly translate in improved ability to detect weak features and/or increase the lower detection limit. However, efforts to increase the surface area of the particles beyond the 18-22 m^2/g by altering reaction conditions with chelating agents met with little success. Clearly a completely different approach would be needed.

One possible route we explored uses emulsion-based synthesis. In this case, the condensation reaction occurs in the aqueous phase inside a water-in oil emulsion. In essence, the surfactant stabilized water droplet behaves as a micro-reactor in which the condensation and hence growth in particle is limited by its size. The size of the droplet is in the submicron to micron range at this size provides a potential means for substantially increasing the surface area of m-WO_3 particles. Furthermore, the individual particles would be encapsulated by surfactant and this should sterically restrict the amount of sintering occurring in the calcination step. While this approach has been used to synthesize sol-gel particles of SiO_2[47] and TiO_2[48], to the best of our knowledge, it has not been used to fabricate WO_3 based particles.

There is a second reason that attracted us to establishing a research effort in surfactant based synthesis of metal oxide materials. It is our intent to leverage the

experience gained from work with surfactant driven synthesis of nano-particulates to develop "designer" nanocomposite material with structural control extending to micron dimensions. Materials composed of oxides, sulfides, phosphates have been made in this manner using liquid crystalline surfactants and phase separated block copolymers to template the assembly of the inorganic framework.[71] The long range goal is to develop WO_3 based material that have an additional lever of size selectivity for application in detection, filtering and decomposition of N-, S- and P- organo compounds. The idea is based on biomimetic materials chemistry, in which organic and inorganic precursors are co-assembled into composite materials with molecular level command over interfaces, structure and morphology.

4.2 Preparation of tungsten trioxide using W/O emulsion

4.2.1 Preparation of the W/O emulsion

A W/O emulsion is composed of continuous phase containing solvent, micro-water-droplets, micelles and free surfactant. (see figure 4.1)

The conditions leading to droplet-stabilized emulsions for polymerization reactions depends on parameters such as the type and concentration of surfactant, the surfactant/water/organic solvent ratio, the rate of stirring and temperature.[57] In our case, we are limited to nonionic surfactant systems as traditional cationic or anionic surfactants are salts. These salts have counter ions such as Na^+ or Cl^- and their presence would lead to mixed tungstates.

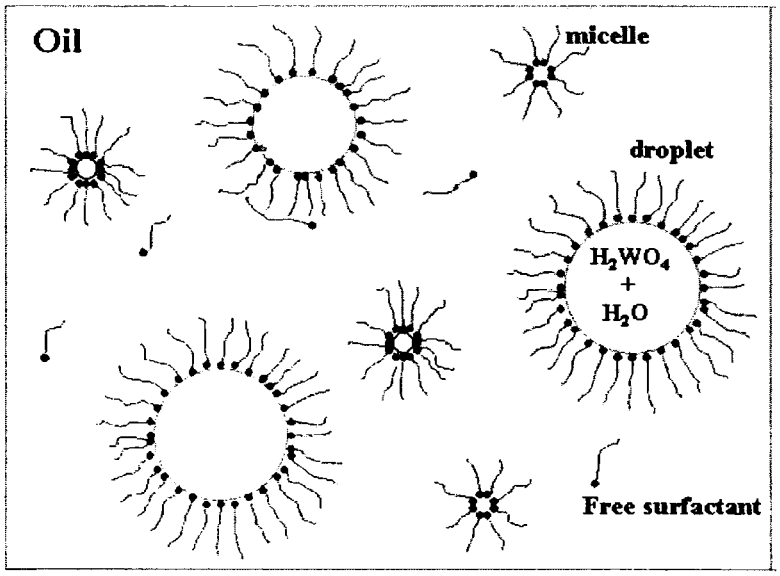

Figure 4.1 Micelles and droplets in the emulsion

The choice of surfactants is based upon their HLB (hydrophilic-lipophilic balance) value and this should be between 3~6 for a W/O emulsion. The HLB values have been tabulated for a number of surfactants and for our research we have selected two non-ionic surfactants, Span-60 and Span-80 dissolved in toluene. This system has been used to generated w/o emulsions.[72]

The structures of Span-60 and Span-80 are shown below:

Sorbitan monostearate

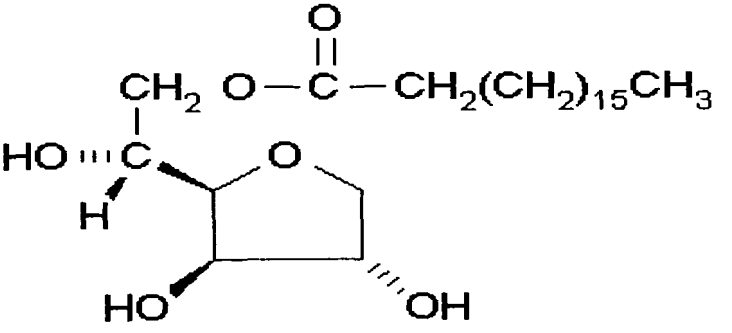

Figure 4.2 Structure of Span-60 ($C_{24}H_{46}O_6$) HLB = 4.7

Sorbitan monooleate

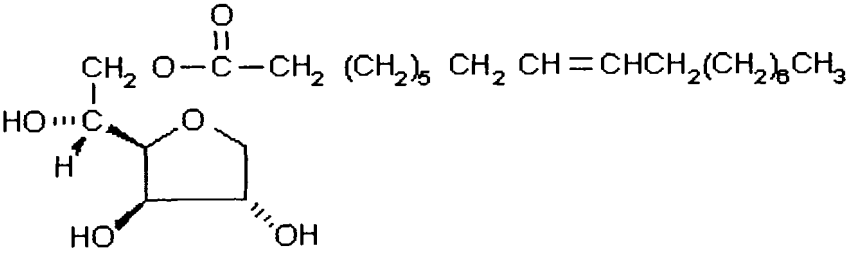

Figure 4.3 Span-80 ($C_{24}H_{44}O_6$) HLB = 4.3

The primary difference between Span-60 and Span-80 is that Span 80 contains an unsaturated aliphatic tail. Span-60 is a solid at room temperature while Span-80 is a highly viscous liquid.

The main factor influencing the micelle size and droplet size is the molar ratio of water/surfactant (R). When the concentration of the surfactant in the solvent is higher than the CMC (critical micelle concentration), stable emulsion are formed with micelles containing 50-100 surfactant molecules and the size of 4-6 nm.[73] Micron-sized water droplets are also formed in the emulsion, the size of these droplets are determined by the molar ratio of water/surfactant and is influenced by the stirring rate. In general, the more vigorous the stirring, the smaller the droplets. As the sol-gel reaction of tungstic acid occurs in the aqueous phase, the growth of the tungsten trioxide hydrate was then limited by the size of the droplet. The size of the droplet can be adjusted by changing the parameters for the emulsion, such as solvent, type of surfactant, temperature, and the water/surfactant/solvent concentration ratio.

4.2.2 Preparation of water/surfactant/toluene emulsion

The surfactant/toluene ratio was first prepared by dissolving a known quantity of Span-60 or Span-80 in 200 ml of toluene. The water/surfactant /toluene ratio was determined by adding the tungstic acid exiting the ion –exchange column directly into a vessel containing the surfactant/toluene at a rate of about 0.5ml/min. During the addition of the tungstic acid, the surfactant/toluene was vigorously stirred at 1000~1600 rpm. In some experiments the concentration of tungstic acid added to the surfactant/toluene was varied. The concentration of tungstic acid was adjusted by changing the concentration of the $Na_2WO_4.2H_2O$ solution added to the top of the ion-exchange column. In all cases, the addition of the aqueous solution caused an immediate clouding of the stirred surfactant/toluene solution indicative of the formation of an emulsion.

The high-speed stirring continued for 5 minutes after the addition of tungstic acid followed by a gentler magnetic stirring (300-rpm) for the following 72 hours. During the entire stirring, a single cloudy phase suspension was observed. The emulsion was then left to sit in a sealed container for an additional 48 hrs to ensure complete reaction.

Removal of the water and toluene was accomplished by evaporation to dryness at room temperature. This typically required 24 hrs. During the evaporation, the water/surfactant/toluene ratio is constantly changing and a different behavior was observed for the Span-60 and Span-80 based systems. In the Span-60 based systems, a clear upper phase (toluene) appeared and the lower phase remained cloudy. The lower cloudy phase remained until removal of all solvent. In the case of Span-80 based systems, as the evaporation proceeded, three phases appeared; an upper toluene phase, a middle cloudy slice, and a lower aqueous phase region.

In order to remove the surfactant, and to convert the hydrated tungsten oxide to m-WO_3, the powder was calcined at 500°C. Samples were transferred to a furnace, heated to 500°C at a rate of 2°C/min and kept at that temperature for 6 hours, and then cooled to room temperature at a rate of 20°C/min. The oxidation of the surfactant at 500°C was more difficult to accomplish than observed for the removal of the chelating agents. In some samples, particularly high surfactant loading, removal of the surfactant required prolonged heating at higher temperatures.

4.3 Results and discussion

4.3.1 Emulsion using Span-60

Table 4.1 Different amount of surfactant

Sample	Toluene (ml)	Span-60 (g)	C- elutant (M)	V- elutant (ml)	Surface area (m^2/g)
L1	200	5	0.12	20	20.7
L2	200	10	0.12	20	45.6
L3	200	20	0.12	20	42.7

In the first experiment the toluene volume as well as the tungstic acid concentration and volume were held constant and the amount of Span-60 was varied. In principle, the higher the surfactant concentration, the smaller the droplets size.[57] The measured surface area of the m-WO_3 particles obtained using three surfactant amounts is given in Table 4.1. There is a notable increase in surface area for the emulsion-based synthesis over those obtained using chelating agents. The lowest surface area obtained using emulsions were on par with the best materials obtained using chelating agents. There was a substantial increase in surface area by doubling the surfactant concentration from 5 g to 10 g and this value leveled with little increase in surface area by adding more surfactant. In actuality there is a drawback to using too much surfactant, as it was difficult to oxidize and remove the excess surfactant prepared using 20 g of span-60.

In the next experiment we examined the effect of lowering the amount of tungstic acid in the system. This can be accomplished by decreasing the concentration of the

tungstic acid. Given that the droplet sized is fixed, a decrease in concentration limits the particle growth because the amount of tungstic acid per droplet is lowered. The surface area obtained for these samples are labeled M1-M3 in table 4.2.

Table 4.2 Different concentration of tungstic acid

Sample	Toluene (ml)	Span-60 (g)	C- elutant (M)	V- elutant (ml)	Surface area (m^2/g)
M1	200	10	0.12	20	45.5
M2	200	10	0.06	20	29.9
M3	200	10	0.03	20	27.4

Our results show that a lowering in concentration in tungstic acid does not lead to particles with higher surface area. An explanation for this trend is provided in the next paragraph.

Experiments were then conducted where the volume of tungstic acid was reduced (see samples N1-N3 in table 4.3)

Table 4.3 Different volume of tungtic acid

Sample	Toluene (ml)	Span-60 (g)	C- elutant (M)	V- elutant (ml)	Surface area (m^2/g)
N1	200	10	0.12	20	45.5
N2	200	10	0.12	10	60.0
N3	200	10	0.12	5	7.3

This produced mixed results with samples varying in surface area from 60 m^2/g to 7.2 m^2/g. Examination of the samples by Raman spectroscopy showed that the samples prepared with lower concentration or lower volume of tungstic acid contained a significant amount of hydrated tungsten oxide. This was a common feature found for samples that have high surfactant to tungstic acid ratios (i.e., increase surfactant loading or lower tungstic acid amount). In order to convert the samples to m-WO_3 we found that we needed to heat the samples to a higher temperature of 550°C for a longer time of 12 hours. Heating at this higher temperature caused a large reduction in surface area as shown in Table 4.4.

Table 4.4 Change of surface area

Sample	Surface area (m^2/g)	Surface area 12 hrs after 550°C (m^2/g)
N1	45.5	13.4
N2	60.0	17.4

The optimum compromise between these variables is associated with sample L2 yielding m-WO_3 particles with surface area of about 45 m^2/g.

4.3.2 Emulsion using Span-80

The surface area measured for samples prepared using span-80 are shown in Table 4.5. In these samples the volume of toluene and tungstic acid were held constant and the amount of surfactant was varied. All samples produced surface areas much below

those obtained with Span 60 or with oxalate chelating agent. We attribute this lower surface area to the three-phase separation leading to an aqueous phase during the drying stage. One of the principle roles of the surfactant or chelating agent is to prevent aggregation and sintering during the calcination stage. With Span 80 the solvent evaporation leads to the loss of stabilized water droplets and an aqueous phase containing the hydrated tungsten oxide appears. The particles aggregate to larger structures with few surfactant molecules available to sterically prevent sintering upon calcination.

Table 4.5 Effect of the amount of Span-80

Sample	Toluene (ml)	C-elutant (M)	V-elutant (ml)	Span-80 (g)	Surface area (m^2/g)
O-1	200	0.1213	10	5	9.7
O-2	200	0.1213	10	10	3.8
O-3	200	0.1213	10	20	13.0
O-4	200	0.1213	10	40	3.3

4.4 Conclusion

Monoclinic WO_3 particles with surface areas of 45 m^2/g have been synthesized using nonionic surfactants. This represents an increase by a factor of 2 over the best materials obtained using oxalate chelating agents. A particle of 45 m^2/g is equivalent to a 17 nm diameter particle size and this is on par with the smallest particles of metal oxides produced by solution based synthetic methods. While the optimum conditions have not been identified, it is clear that there is a need to avoid the use of high surfactant to tungstic acid ratio as this leads to difficulty in removing the surfactant in the calcination

of hydrated tungsten oxide to m-WO_3. An important role for both chelating agents and surfactant is that they play a significant role in minimizing the sintering occurring in the calcination step.

Chapter 5

IDENTIFICATION OF SURFACE SITES ON NANO-SIZED MONOCLINIC WO_3 POWDERS BY FT-IR SPECTROSCOPY

5.1 Introduction

Before embarking on gas phase adsorption studies with these high surface area particles described in chapters 3 and 4, there is a need to first identify the reactive groups present on the m-WO_3 surface at various evacuation temperatures. This is important because the degree of surface hydroxylation/hydration and hence, the number of exposed Lewis acid and base sites on metal oxides can be altered by evacuation at elevated temperature. As a consequence, evacuation temperature plays a critical role in defining the surface reactions and surface species formed in subsequent reactions of gaseous molecules with the metal oxide surface.

While there are numerous infrared studies devoted to monitoring the dehydroxylation/dehydration behavior as a function of temperature on many oxides[61], we are not aware of similar studies on monoclinic WO_3 (m-WO_3) powders. Typically, the identification of surface sites on metal oxide powders is largely based on the ability to detect infrared bands due to various hydroxyl groups (both from adsorbed water and surface M-OH modes) and by using the position of bands of adsorbed molecules such as pyridine to probe Lewis acid/Brønsted acid site densities. Bands due to adsorbed water on $WO_3 \cdot 2H_2O$ and NH_3 adsorption on sputtered tungsten oxide films have been detected,[62,63] but these studies were on amorphous WO_3 based material before crystallization into the stable monoclinic form.

5.2 Experimental section

Two methods were used to record IR spectra. We used Diffuse Reflectance (DRIFT) on the neat powder in order to detect the relatively weak IR bands due to adsorbed water and surface hydroxyl groups in the dehydroxylation/dehydration experiments. Although it was possible to record transmission spectra using self-supporting disks, we found that this method was not practical because the disks were fragile and therefore difficult to fabricate for routine use. Drift spectra were recorded using a Harrick preying mantis equipped with an environmental chamber on neat m-WO_3 powders. A DRIFT reference spectrum was recorded using KBr powder.

The adsorption of pyridine was recorded in transmission using a thin film of m-WO_3 powder dispersed on a KBr window. Details of the thin film technique are described elsewhere.[68] The thin film technique enabled detection of bands due to adsorbed species across the entire infrared region. This was important for detection of bands that lie in the same region as the strong bulk modes (1300 to 970 cm^{-1}).

In the thin film experiments, difference spectra are plotted with the reference spectrum recorded using the thin film m-WO_3 previously evacuated at the specified temperature and cooled to room temperature. The difference spectrum was recorded after addition of the pyridine at room temperature for 5 minutes, followed by evacuation for 2 minutes. Positive bands are due to bonds that formed on the surface and negative bands represent bond removal from the surface.

5.3 Results and discussion

5.3.1 Dehydration of m-WO_3

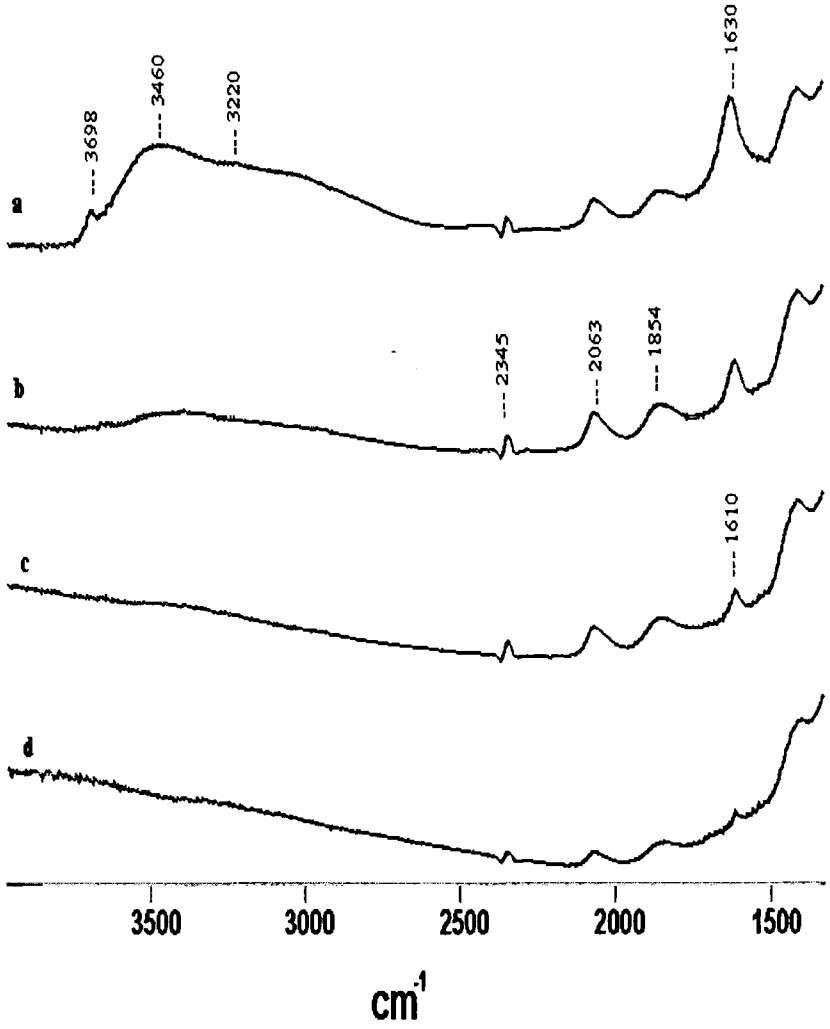

Figure 5.1 Infrared spectra of the m-WO_3 powder evacuated at various temperatures (a) RT, (b) 150 °C, (c) 300 °C , and (d) 400 °C

Figure 5.1 shows the DRIFT infrared spectra of the m-WO_3 sample recorded in air at room temperature (Figure 5.1a) and evacuated at various temperatures (Figures 1b-d). The region below 1300 cm^{-1} is not shown because it is opaque due to the presence of strong W-O bulk modes. Bands located at 2063 and 1854 cm^{-1} do not change with evacuation and are therefore assigned to various overtone and combination W-O bulk modes. The region between 3800 to 3000 cm^{-1} contains bands due to both surface WOH and adsorbed water. Since this section is devoted to dehydration and not dehydroxylation, we first describe the trends observed for the H_2O bending mode located at 1630 cm^{-1} because this band is unique to the presence of adsorbed water on the surface. By monitoring the change in intensity of the bending mode at 1630 cm^{-1} it is possible to determine the degree of dehydration of the m-WO_3 with evacuation temperature. This curve is shown in Figure 5.2. The ordinate value is calculated from the integrated peak areas at 1630 cm^{-1} ratioed to the m-WO_3 bulk mode at 2063 cm^{-1}.

The shape of the curve in figure 5.2 is very similar to the weight loss curve in a thermal programmed desorption experiments on amorphous hydrated tungsten hydroxy oxide ($WO_x(OH)_y \cdot H_2O$) films[62,74]. On the amorphous material, there is a large initial decrease in weight that tapers to zero at about 150 °C followed by a second smaller decrease in weight between 300 and 350 °C. Both weight loss were due to elimination of water and it was concluded that the initial weight loss below 150 °C was due to removal of adsorbed molecular water and the second decrease in weight beginning at 300 °C was from condensation of adjacent surface WOH groups.

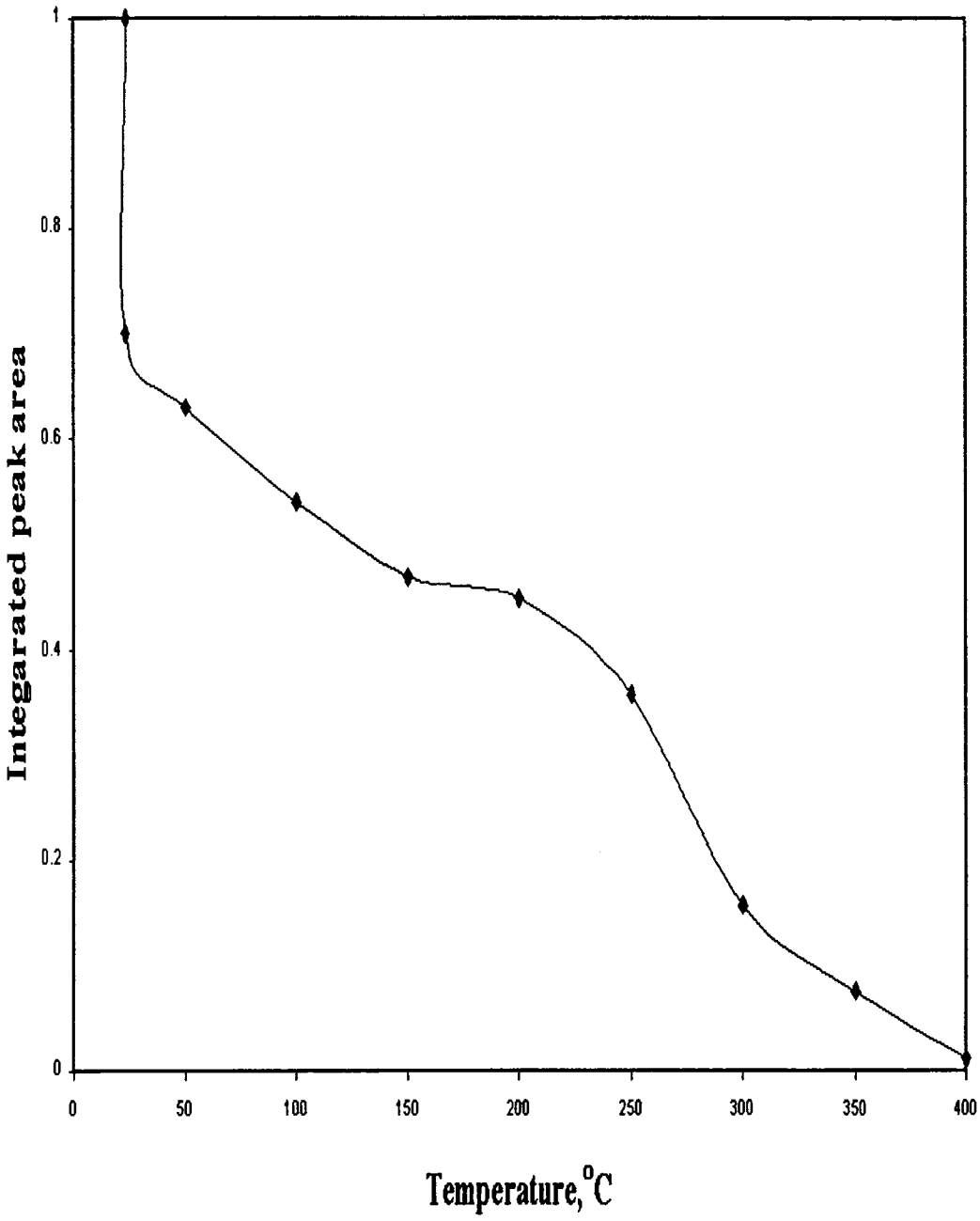

Figure 5.2 Desorption of water from m-WO_3 surface as a function of evacuated temperatures.

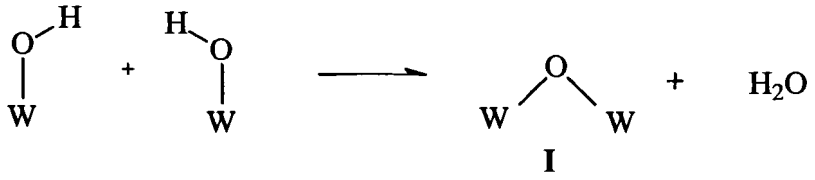

I

In our case, the data shown in figure 5.2 is derived from the bending mode of water and thus, the second decrease at 350 °C is due to water removal and not WOH condensation. This shows that there are two types of adsorbed water on the surface. Most of the adsorbed water is weakly bound to the surface and eliminated with evacuation at 150 °C. A second type of adsorbed water remains on the surface and is eliminated only after evacuation at temperatures above 350 °C.

One possible explanation for the presence of adsorbed water above 150 °C is that it is caged in the microporous structure of the oxide. Evidence supporting a caged explanation is provided by the sharp band at 2345 cm^{-1} that appears in all curves in Figure 5.1. This band at 2345 cm^{-1} is due to weakly adsorbed CO_2 and this band persists even with evacuation at 400 °C. A similar finding has been obtained for a fumed silica immersed in supercritical CO_2.[75] Although CO_2 does not adsorb on silica, the high pressure (200 bar) used in the supercritical experiments forced some CO_2 into the micropores or interstitial regions within the silica structure. This caged CO_2 gave rise to a characteristic infrared band at 2338 cm^{-1} and was not removed by simple evacuation at elevated temperature. Therefore we conclude that the CO_2 observed in the m-WO_3 spectra in figure 5.1 is also due to CO_2 entrapped in the m-WO_3 powder. We note that in order to obtain small m-WO_3 particles suitable for infrared studies, oxalate and acetate

chelating agents or nonionic surfactants are used in the sol-gel synthesis. The band at 2345 cm^{-1} is not observed when the m-WO_3 sol-gel powders are synthesized in the absence of oxalate/acetate chelating agents or by emulsion polymerization using nonionic surfactants. The most likely explanation is that the water and CO_2 produced from the combustion of the organic oxalic/acetic acid precursors or surfactants become trapped during the annealing the m-WO_3 powders at 500 °C. Given that there is trapped CO_2, it is expected that a fraction of the adsorbed water is also embedded inside the sol-gel powder.

Additional experimental evidence shows that the contribution due to trapped water is small and cannot account for the loss of water between 350 and 400 °C. For example, we find that the m-WO_3 that is evacuated at 400 °C completely rehydrates upon exposure to air at room temperature. Perhaps the most convincing evidence is provided by D_2O exchange experiments at room temperature. If the elimination of water above 350 °C was due to inaccessible or trapped water then these molecules should not readily exchange with addition of D_2O vapor at room temperature.

Figures 3a and b show the infrared spectra of the m-WO_3 thin film before and after the exposure to D_2O for 15 minutes at room temperature, respectively. There is almost a complete disappearance of the OH modes in the 3600-3200 cm^{-1} along with the H_2O band at 1630-1610 cm^{-1} and this is accompanied by the appearance of infrared bands at 2710, 2539, and 2266 cm^{-1}. This clearly shows that the D_2O easily accesses all the water / WOH groups at room temperature.

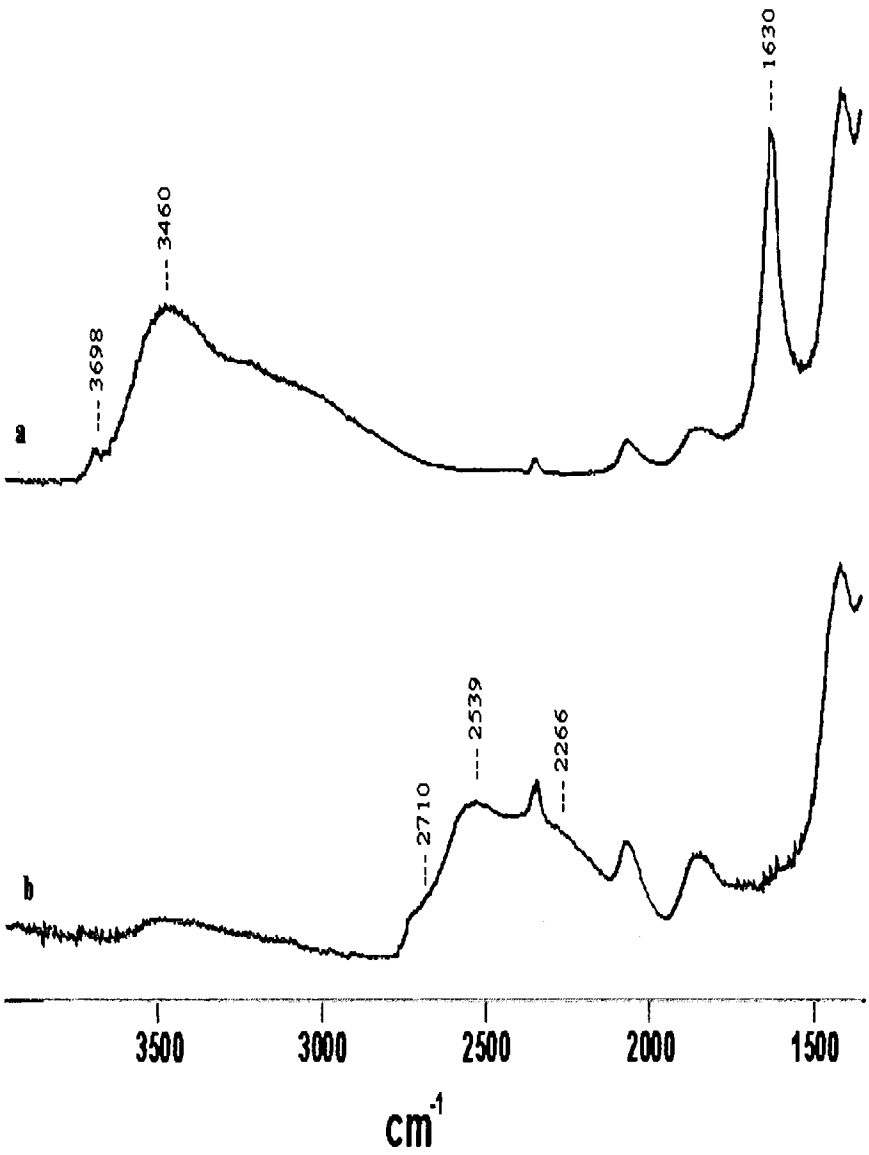

Figure 5.3 Infrared spectra of a) m-WO_3 powder and b) after addition of the D_2O vapor for 15 minutes at room temperature followed by evacuation for 2 minutes.

Only a weak band at 3500 cm^{-1} remains showing that only a very small fraction of the adsorbed water is due to entrapped water from the combustion of the organic oxalate/acetate ligands or surfactants in the sol-gel synthesis. This trapped amount of water cannot account for the decrease in water observed between 350 and 400 °C in curve 2. Moreover, the rapid exchange of the WOH groups attests to the high lability or acidity of the hydroxyl groups. Other oxides such as alumina, titania and silica usually require multiple exposures of D_2O vapor at elevated temperatures to achieve high exchange levels of the surface OH to OD groups.[76]

There is spectroscopic evidence supporting both a strong and weakly bound water on the surface. Below 150 °C the bending mode is located at 1630 cm^{-1} and this band shifts and appears at 1610 cm^{-1} at evacuation temperatures at 150 °C and above. A band at 1630 cm^{-1} is attributed to a weakly held hydrogen bonded water layer similar to that found on oxides such as silica.[75] The second more strongly adsorbed water has a band at lower frequency (i.e., 1610 cm^{-1}) and this suggests that it is adsorbed through the oxygen atom of the water through coordination with Lewis sites (structure II).

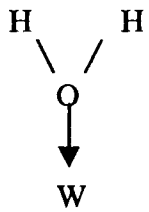

II

In support of this assignment, it is noted that a shift to lower frequency in the H_2O bending mode has been observed at 1609 cm^{-1} for hydrated $WO_3.{}^1/_3H_2O$ and this was assigned to water H-bonded through the oxygen atom of the water molecule.[63]

In making m-WO_3 via the sol-gel route, the hydrated $WO_3.2H_2O$ produced in the polymerization process is converted to m-WO_3 by calcination at 500 °C. While the dominant composition of the material is m-WO_3, there would remnants of the amorphous ($WO_x(OH)_y{\cdot}H_2O$) still present. Thus, it is plausible that the more strongly bound H_2O is associated with a covalent type W—OH_2 species of the residual amorphous material.

5.3.2 Dehydroxylation of m-WO_3

The OH stretching region contains a sharp band at 3698 cm^{-1} and two broad bands centered at 3460 and 3220 cm^{-1}. The change in intensity of the 3460 cm^{-1} band differs from the 3698 cm^{-1} and 3220 cm^{-1} bands and mirrors the change in intensity of the 1630 cm^{-1} band. Therefore, the band at 3460 cm^{-1} is due to the weakly adsorbed water layer associated with the bending mode at 1630 cm^{-1}. On oxides such as alumina, titania, and silica isolated surface hydroxyl groups produce sharp bands in the 3750-3600 cm^{-1} region and hydrogen bonded hydroxyl groups give rise to broad bands between 3400-3000 cm^{-1}.[61] Based on this trend, we assign the band at 3698 cm^{-1} to isolated WOH and the broad band centered at 3220 cm^{-1} to hydrogen bonded WOH groups. The isolated WOH band is completely eliminated and the hydrogen bonded WOH groups show a large decrease with evacuation at room temperature (see Figure 5.1).

While this level of dehydroxylation with ambient evacuation is large when compared to alumina or titania, it is noted that m-WO_3 is more easily reduced with evacuation or heating than the other oxides. The reduction of m-WO_3 is most often associated with the loss of lattice oxygen resulting in a change in conductivity and optical transparency of the oxide.[77,78] However, with the high surface area sol-gel particles, a

significant fraction of the loss of oxygen is associated with removal of surface hydroxyl groups. It is noted that this does not preclude the loss of lattice oxygen in the sol-gel particles as we do observe a decrease in overall transparency of the oxide that increases with evacuation temperature.[79,80]

Between 150 and 400 °C there is a continual decrease in the broad band between 3500 and 3100 cm^{-1} with a higher degree of erosion on the low frequency side. At 400 °C there remains a weak broad band centered at about 3500 cm^{-1}. The gradual decrease with evacuation of the low frequency side of the broad band between 3500 and 3100 cm^{-1} at temperatures of 150 to 400 °C shows that further reduction in surface OH groups arises from condensation of the strongest H-bonded WOH groups. The remaining broad band near 3500 cm^{-1} is most likely due to inaccessible or trapped H_2O/OH groups. In the exchange experiment with D_2O we find a small but detectable broad band at 3500 cm^{-1} that is resistant to exchange with D_2O.

5.3.3 Adsorption of pyridine

Adsorption on metal oxide surfaces occurs primarily with the surface hydroxyl groups, the adsorbed water layer and Lewis acid/base sites. On oxides such as titania and alumina, dehydroxylation leads to the creation of coordinatively unsaturated Lewis acid and base sites.[61]

III

Pyridine is a common probe molecule to monitor the adsorption sites on metal oxide surfaces.[81-84] Adsorbed pyridine shows different and characteristic infrared bands depending on whether the pyridine form hydrogen bonds (IV), form a pyridium ion via proton transfer with the acidic surface hydroxyl groups (V) or is coordinated to a Lewis acid site (VI). The three types of bonding are shown in Scheme 1 below.

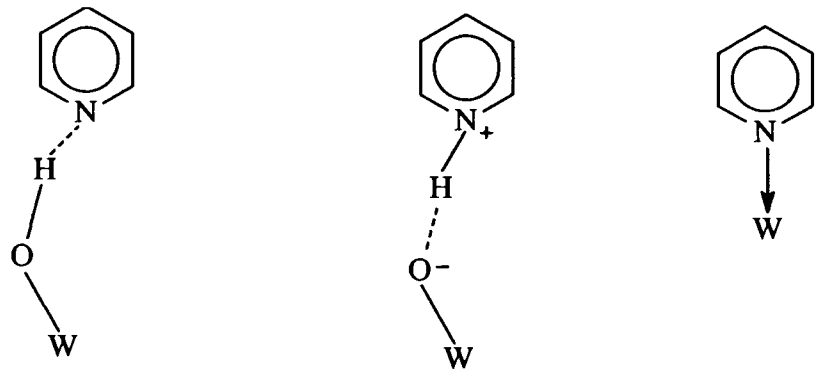

IV **V** **VI**

Scheme 1

Clearly the number and type of sites will vary with the degree of dehydroxylation/dehydration of the surface. Given the dehydration behavior shown in Figure 5.2, we selected three evacuation temperatures of the m-WO_3 to be probed by the adsorbed pyridine. Specifically, the pyridine was added to a highly hydrated/hydroxylated m-WO_3 thin film evacuated at room temperature and a partially

and fully dehydrated/dehydroxylated m-WO_3 samples evacuated at 150 and 400 °C, respectively. The spectra are shown in Figure 5.4.

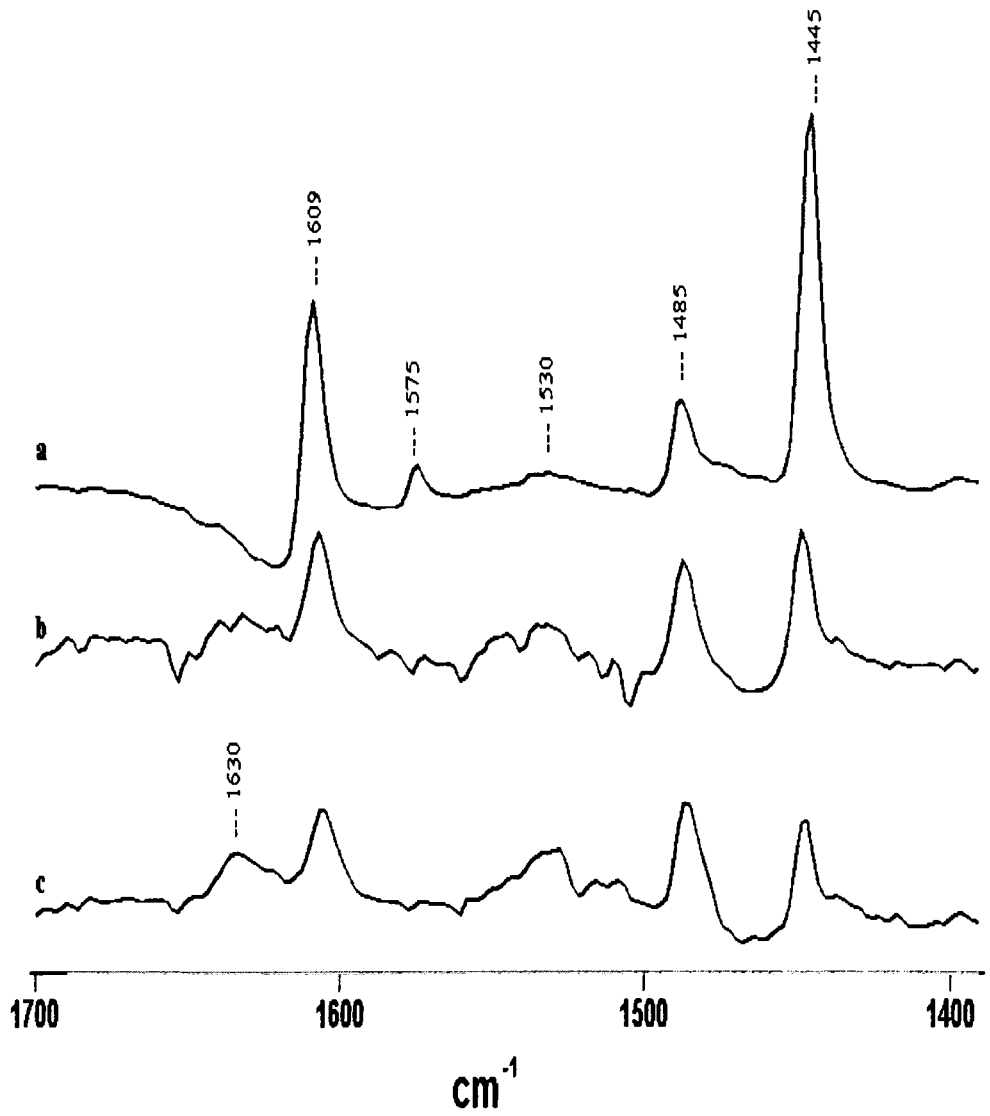

Figure 5.4 Infrared spectra of pyridine adsorbed at room temperature on m-WO_3 evacuated at (a) room temperature (b) 150 °C, and (c) 400 °C

For all three samples, excess quantity of pyridine vapor was added for 5 minutes at room temperature, followed by evacuation for 2 minutes. The spectrum obtained for pyridine addition to m-WO_3 evacuated at room temperature (Figure 5.4a) is dominated by bands at 1609, 1575, 1485 and 1445 cm^{-1} characteristic of coordination to Lewis acid sites.[85,86] Figure 5.4a also shows a weak band at 1530 cm^{-1} assigned to the pyridium ion showing that a few WOH groups are acidic in nature. In addition, all bands in the OH stretching region and the H_2O bending mode are significantly reduced in intensity (spectrum not shown). The elimination of water and OH sites gives rise to Lewis coordinated pyridine. This result is similar to that observed on TiO_2 and is evidence of the ionic characteristic of the vast majority of the OH groups and coordinated water to W Lewis sites.[81,82] In essence, the water is adsorbed as coordinating ligands rather than through hydrogen bonding interactions with the surface WOH groups[87] and the pyridine is a better nucleophile than the surface OH_2 groups and easily displaces them from the surface:

$$W\text{-}OH_2 + Py \longrightarrow W\text{-}Py + H_2O$$

For m-WO_3 evacuated at 150 °C, the amount of pyridine adsorbed with Lewis acid sites is reduced by a factor of three relative to the sample evacuated at room temperature while the number of Brønsted coordinated species (band at 1530 cm^{-1}) remain constant. This result clearly shows that the removal of OH groups (presumably through condensation of adjacent WOH groups) and coordinated H_2O reduces the number of Lewis sites available for adsorption of pyridine. This contrasts to the picture

shown in scheme 1 where removal of surface hydroxyl groups exposes Lewis acid sites on the surface. One possible explanation is that the site vacated by the removal of surface OH groups and H_2O is replaced by the migration of lattice O^{-2} sites from the bulk. The O^{-2} would be a poorer leaving groups than an OH^- or H_2O and would lower the Lewis acidity of coordinatively unsaturated sites. We recall that evacuation at elevated temperature reduces the transmission of the m-WO_3 and this has been attributed to the creation of vacancies in the titanium conduction band arising from the extraction of lattice oxygen.[77] The number of Brønsted sites remains essentially constant between evacuation at room temperature and 150 °C. This is consistent with the presence of small quantities of hydrated amorphous WO_3. The hydrated WO_3 is converted to m-WO_3 with heating only at temperatures above 400 °C.

The spectrum obtained for pyridine adsorption on m-WO_3 evacuated at 400 °C showed minor changes when compared to the spectrum of obtained for an evacuated sample at 150 °C. The number of Lewis sites is slightly lower and the number of Brønsted sites (bands at 1630 and 1530 cm^{-1}) is slightly higher for the 400 °C evacuated sample. This shows that the major changes in the number and type of surface sites (hydration, hydroxylation and Lewis acid) occur between ambient and 150 °C. The slight increase in Brønsted acidity occurring at 400 °C is attributed to the dehydration of the amorphous WO_3 which results in an increase in acidity of the remaining hydroxyl group on the partially hydrated material.

5.4 Conclusion

The surface of m-WO_3 contains both free and hydrogen bonded hydroxyl groups as well as a layer of adsorbed water coordinated to Lewis acid sites. Both the adsorbed water and hydroxyl groups are easily removed by evacuation at 150 °C. The total number of adsorption sites is reduced by the removal of the hydroxyl groups and coordinated water, as their removal does not result in the exposure of Lewis sites on the surface. Between 150 and 400 °C the number and type of surface sites remain essentially unchanged.

REFERENCES

(1) Zemel, J. N. *Thin Solid Films* **1988**, *163*, 189.

(2) Ylilammi, M. *Sens. Actuators* **1989**, *18*, 167.

(3) Lalauze, R.; Pijolat, C. *Sens. Actuators* **1984**, *5*, 55.

(4) Gopel, W. *Sens. Actuators B* **1989**, *16*, 167.

(5) Shaver, P. J. *Appl. Phys. Lett.* **1967**, *11*, 255.

(6) Macintyre, J. R.; Marshall, T. N. *Instrumentation technology* **1972**, *8*, 29.

(7) Wohltjen, H.; Dessy, R. *Anal. Chem.* **1979**, *51, No.9*, 1458.

(8) Xu, C.; Tamaki, J.; Miura, N.; Yamazoe, N. *Sens. Actuators B* **1991**, *3*, 147.

(9) Berberich, M.; Zheng, J. G.; Weimar, U.; Gopel, W.; Barsan, N.; Pentia, E.; Tomescu, A. *Sens. Actuators B* **1996**, *31*, 71.

(10) Depero, L. E.; Ferroni, M.; Guidi, V.; Marca, G.; Martinelli, G.; Nelli, P.; Sangaletti, L.; Sberveglieri, G. *Sens. Actuators B* **1996**, *35-36*, 381.

(11) Jin, Z.; Zhou, H.; Jin, Z.; Savinell, R.; Liu, C. *Sens. Actuators B* **1998**, *52*, 188.

(12) Dong, L. F.; Cui, Z. L.; Zhang, Z. K. *Nano-structured material* **1997**, *8*, 815.

(13) Rickerby, D. G.; Horrillo, M. C.; Santos, J. P.; Serrini, P. *Nano-structured material* **1997**, *9*, 43.

(14) Lin, H.; Keng, C.; Tung, C. *Nano-structured material* **1997**, *9*, 747.

(15) Rickerby, D. G.; Horrillo, M. C. *Nano-structured material* **1998**, *10*, 357.

(16) Willett, M.; Burganos, V.; Tsakiroglou, C.; Payatakes, A. *Sens. Actuators B* **1998**, *53*, 76.

(17) Bechinger, C.; Muffler, H.; Schafle, C.; Sundberg, O.; Leiderer, P. *Thin Solid Films* **2000**, *366*, 135.

(18) Brinker, C. J.; Scherer, G. W. *The Physics and Chemistry of Sol-Gel Processing Academic Press, New York* **1990**.

(19) Bradley, D. C.; Mehrotra, R. C.; Gaur, D. P. *Metal Alkoxides Academic Press, London* **1978**.

(20) Hubert-Pfalzgraf, L. G. *New Journal of Chemistry* **1987**, *11*, 663.

(21) Penza, M.; Vasanelli, L. *Sens. Actuators B* **1997**, *41*, 31.

(22) Cantalini, C.; Pelino, M.; Sun, H. T.; Faccio, M.; Santucci, S.; Lozzi, L.; Passacantando, M. *Sens. Actuators B* **1996**, *35-36*, 112.

(23) Sun, H.; Cantalini, C.; Lozzi, L.; Passacantando, M.; Santucci, S.; Pelino, M. *Thin Solid Films* **1996**, *287*, 258.

(24) Lee, K. *Thin Solid Films* **1997**, *302*, 84.

(25) Cantalini, C.; Wlodarski, W.; Li, Y.; Passacantando, M.; Santucci, S.; Comini, E.; Faglia, G.; Sberveglieri, G. *Sens. Actuators B* **2000**, *64*, 182.

(26) Cantalini, C.; Atashbar, M. Z.; Li, Y.; Ghantasala, M. K.; Santucci, S.; Wlodarski, W.; Passacantando, M. *J. Vac. Sci. Technol.* **1999**, *A17*, 1873.

(27) Bessiere, A.; Badot, J.; Certiat, M.; Livage, J.; Lucas, V.; Baffier, N. *Electrochimica Acta* **2001**, *46*, 2251.

(28) Tong, M; Dai, G.; Gao, D. *Mater. Chem. and Phys.* **2001**, *69*, 176.

(29) Nenadovic, M.; Rajh, T.; Micic, O.; Nozik, A. *J. Phys. Chem.* **1984**, *88*, 5827.

(30) Music, S.; Vertes, A.; Simmons, G. W; Czako-Nagy, I. *J. Colloid Interface Sci.* **1982**, *85*, 256.

(31) Gotic, M.; Popovic, S.; Ljubesic, N.; Music, S. *J. Mater. Sci.* **1994**, *29*, 2474.

(32) Chemseddine, A.; Morineau, R.; Livage, J. *Sol. St. Ionics* **1983**, *9 & 10*, 357.

(33) Gotic, M.; Ivanda, M.; Popovic, S.; Music, S. *Mater. Sci. and Eng. B* **2000**, *77*, 193.

(34) Namba, T.; Nishiyama, Y.; Yasui, I. *J. Mater. Res.* **1991**, *6*, 1324.

(34) Daniel, M. F.; Desbat, B.; Lassegues, J. C.; Gerand, B.; Figlarz, M. *J. Sol. St. Chem.* **1987**, *67*, 235.

(36) Pigeat, P.; Pacia, N.; Weber, B. *Surf. Sci.* **1992**, *269 & 270*, 538.

(37) Sun, M; Xu, N.; Cao, Y. W.; Yao, J. N.; Wang, E. G. *J. Mater. Sci. Lett.* **2000**, *19*, 1407.

(38) Deepa, M.; Sharma, N; Varshney, S; Varma, S.; Agnihotry, S. A. *J. Mater. Sci.* **2000**, *35*, 5313.

(39) Livage, J.; Henry, M.; Sanchez, C. *Prog. Solid St. Chem.* **1988**, *18*, 259.

(40) Nishide, T.; Mizukami, F. *Thin Solid Films* **1995**, *259*, 212.

(41) Xu, N.; Sun, M.; Cao, Y. W.; Yao, J. N.; Wang, E. G. *Appl. Surf. Sci.* **2000**, *157*, 81.

(42) Boutonnet, M.; Kizling, J.; Stenius, P.; Maire, G. *Colloids and Surf.* **1982**, *5*, 209.

(42) Mittal, K.; Lindman, B.; Lumfimpadio, N.; Nagy, J. B.; Derouane, E. G. *Surfactants in solution*; Plenum; New York, 1986.

(43) Hou, M. J.; Shah, D. O.; Attia, Y. A.; Moudgil, B. M.; Chander, S. *Interfacial phenomena in Biotechnology and Materials Processing*; Elsevier; Amsterdam, 1988.

(45) Chew, C. H.; Gan, L. M.; Shah, D. O. *J. Dispersion Sci. Technol.* **1990**, *11*, 593.

(46) Kon-no, K.; Koide, M.; Kitahara, A. *J. Chem. Soc. Jpn.* **1990**, *6*, 815.

(47) Arriagada, F.; Osseo, K. *J. Colloid Interface Sci.* **1995**, *170*, 8.

(48) Bauer, W.; Tomandi, G. *Ceram. Int.* **1994**, *20*, 189.

(49) Sarikays, Y.; Akine, M. *Ceram. Int.* **1988**, *14*, 239.

(50) Lang, J.; Jada, A. *J. Phys. Chem.* **1988**, *92*, 1946.

(51) Jada, A.; Lang, J.; Zana, R. *J. Phys. Chem.* **1989**, *93*, 10.

(52) Jada, A.; Lang, J.; Zana, R. *J. Phys. Chem.* **1990**, *94*, 381.

(53) Zana, R.; Lang, J. *J. Phys. Chem.* **1991**, *95*, 3364.

(54) Lang, J.; Mascolo, G.; Zana, R.; Luisi, P. *J. Phys. Chem.* **1990**, *94*, 3069.

(55) Lang, J.; Laiem, N.; Zana, R. *J. Phys. Chem.* **1992**, *96*, 4667.

(56) Lang, J.; Lalem, N.; Zana, R. *J. Phys. Chem.* **1991**, *95*, 9533.

(57) Lang, J.; Lalem, N.; Zana, R. *Colloids and Surf.* **1992**, *68*, 199.

(58) Ghiotti, G.; Chiorino, A.; Boccuzzi, F. *Sens. Actuators* **1989**, *19*, 151.

(59) Ghiotti, G.; Chiorino, A.; Pan, W. *Sens. and Actuators B* **1993**, *15-16*, 367.

(60) Jarzebski, Z. M.; Marton, J. P. *J. Electrochem. Soc.* **1976**, *123*, 299.

(61) Morrow, B. A. In *Spectroscopic Analysis of Heterogeneous Catalysts, Part A: Methods of Surface Analysis*; Fierro, J. L. G. ed.; Elsevier; Amsterdam, 1990.

(62) Agrawal, A.; Habibi, H *Thin Solid Films* **1989**, *169*, 257.

(63) Daniel, M. F.; Desbat, B; Lassegues, J. C.; Gerand, B.; Figlarz, M. *J. Solid State Chem.* **1987**, *67*, 235.

(64) Lee, S.-H.; Cheong, H. M.; Ahang, J.-G.; Mascarenhas, A.; Benson, D. K.; Deb, S. K. *Appl. Phys. Lett.* **1999**, *74*, 242.

(65) Forsythe, E. W.; Choong, V.-E.; Le, T. Q.; Gao, Y. *J. Vac. Sci. Technol. A* **1999**, *17*, 3429.

(66) Salje, E. *Acta Cryst.* **1975**, *A31*, 360.

(67) Nonaka, K.; Takase, A.; Miyakawa, K. *Journal of Mater. Sci. Lett.* **1993**, *12(5)*, 274.

(68) Tripp, C. P.; Hair, M. L. *Langmuir* **1991**, *7*, 923.

(69) Mahler, W.; Bechtold, M. F. *Nature* **1980**, 285(5758), 27.

(70) Sun, M.; Xu, N. *J. Mater. Res.* **2000**, *15*, 927.

(71) Asefa, T.; Yoshina, C.; MacLachlan, M.; Ozin, G. *J. Mater. Chem.* **2000**, *10*, 1751.

(72) Kinugasa, T.; Watanabe, K.; Takeuchi, H. *J. Chem. Eng. Jpn.* **1992**, *25, No.2*, 128.

(73) Pillai, V.; Kumar, P.; Multani, M.; Shah, D. *Colloids and Surf. A* **1993**, *80*, 69.

(74) Schlotter, P.; Pickelmann, L. *J. Elect. Mat* **1982**, *11*, 207.

(75) Tripp, C. P.; Combes, J. R. *Langmuir* **1998**, *14*, 7348.

(76) Kanan, S. M.; Tripp, C. P. *Langmuir* **2001**, *17*, 2213.

(77) Gutiérrez-Alejandre, A.; Ramírez, J.; Busca, G. *Langmuir* **1998**, *14*, 630.

(78) Ozer, N.; Lampert, C. M. *Thin Solid Films* **1999**, *349*, 205.

(79) Guinneton, F.; Valmalette, J.; Gavarri, J. R. *Optical Mater.* **2000**, *15*, 111.

(80) Guinneton, F.; Sauques, l; Valmalette, J. C.; Cros, F.; Gavarri, J. R. *J. Phys. Chem. Solid* **2001**, *62*, 1229.

(81) Busca, G. *Catal. Today* **1998**, *41*, 191.

(82) Kung, M. C.; Kung, H. H. *Catal. Rev.-Sci. Eng.* **1985**, *27*, 425.

(83) Lavalley, J. C. *Catal. Today* **1996**, *27*, 377.

(84) Morterra, C; Magnacca, G. *Catal. Today* **1996**, *27*, 497.

(85) Jones, P.; Hockey, J. A. *J. Chem. Soc., Faraday Trans. 1* **1971**, 2669.

(86) Kataoka, T.; Dumesic, J. A. *J. Catal.* **1988**, *112*, 66.

(87) Linsebigler, A. L.; Lu, G.; Yates J. R. J. *Chemical Review* **1995**, *95*, 735.

BIOGRAPHY OF THE AUTHOR

Zhixiang Lu was born in Gaoyou, Jiangsu Province, P.R. China on September 22, 1973. He was raised in Gaoyou and graduated from Gaoyou High School in 1990. He attended the Tongji University and graduated in 1995 with a Bachelor's degree in Polymer Materials. He entered the Macromolecular Science graduate program at Fudan University in the fall of 1995 and graduated in 1998 with a Master's degree. After he worked in Shanghai Genius Advanced Materials Co.Ltd, Zhixiang Lu began his graduate work at the University of Maine, Orono, Maine, in 1999. Zhixiang Lu is a candidate for the Master of Science degree in Chemistry from The University of Maine in August, 2001.